Resource Allocation for Fairness Enhancement in Multicell Vehicular VLC System With Optical IRS: A Cooperative Transmission Approach

Nan An, Fang Yang, *Senior Member, IEEE*, Chang Liu, Ling Cheng, *Senior Member, IEEE*, Jian Song, *Fellow, IEEE*, and Zhu Han, *Fellow, IEEE*

***Abstract*—In multicell downlink vehicular visible light communication (VLC) systems, vehicles at a cell edge experience lower achievable data rates compared with those at a cell center, primarily due to the weaker channel gain and intercell interference, leading to unfairness among vehicles. In this article, a cooperative transmission approach is proposed for a vehicular VLC system with optical intelligent reflecting surface (OIRS) to enhance the max-min fairness of the system by leveraging the additional OIRS-reflected channels and the interference-mitigating capabilities of cooperative transmission. To this end, the system model is established, followed by the formulation of a resource allocation problem aiming at enhancing max-min fairness, in which the minimum achievable data rate among vehicles is optimized. Then, an effective resource algorithm is proposed, transforming the original problem into an equivalent form and subsequently decomposing it into three subproblems, focusing on OIRS assignment, subchannel allocation, and power adjustment, respectively. By employing a block coordinate descent algorithm, the three subproblems are solved iteratively until convergence. In addition, simulation results confirm the improvement in max-min fairness brought by OIRS and the proposed cooperative transmission approach. Moreover, compared with various baselines, the proposed resource allocation algorithm significantly enhances in the max-min fairness for the vehicular VLC system, crucial for this application.**

***Index Terms*—Cooperative transmission, max-min fairness, optical intelligent reflecting surface (OIRS), vehicular visible light communications (VLC).**

I. Introduction

With continuous technological advancement, transportation is evolving toward the intelligent transportation system (ITS), aiming at reducing traffic accidents and improving efficiency. Vehicle-to-everything (V2X) technology supports communication among vehicles and between vehicles and infrastructure, ensuring interoperability among all participants within ITS and providing a foundation for various ITS applications [2], [3]. Consequently, V2X has become a key supporting technology for ITS, attracting widespread attention from researchers.

Currently, two widely used V2X methods are based on radio frequency (RF) communications [4]. However, the RF spectrum has been divided for various services, resulting in spectrum congestion that hinders the ability to satisfy the escalating service demands. Additionally, communication congestion in high-density node scenarios and potential security attacks pose challenges for the evolution of RF-based V2X technology [5]. Visible light communications (VLC) provides high-data rate transmission by utilizing the unregulated broad frequency band of 380 THz to 750 THz, presenting as one of the potential solutions for V2X technology. Compared with RF-based V2X technology, the line-of-sight (LoS) directional transmission of vehicular VLC effectively alleviates interference and makes eavesdropping more difficult [6]. Besides, vehicular VLC employs low-cost light-emitting diodes (LEDs) widely adopted in streetlamps and automobile lamps as access points (APs), thus ensuring its simple deployment in ITS.

As a crucial component of V2X, infrastructure-to-vehicle (I2V) employs streetlamps for downlink information transmission in vehicular VLC. However, the coverage area of a single cell formed by one streetlamp is small, providing illumination and communication for only a few vehicles. In this case, multiple streetlamps arranged along the road can collectively cover vehicles, forming a multicell I2V communication system. Within these cells, a notable discrepancy

Received 27 September 2024; accepted 20 January 2025. Date of publication 13 February 2025; date of current version 23 May 2025. This work was supported in part by the Shenzhen Municipal Government under Grant SZXJP20230703093002006; in part by the Center of National Railway Intelligent Transportation System Engineering and Technology, China Academy of Railway Sciences under Grant 2023YJ361; in part by the National Science Foundation under Grant ECCS-2302469; in part by the Japan Science and Technology Agency (JST) Adopting Sustainable Partnerships for Innovative Research Ecosystem (ASPIRE) under Grant JPMJAP2326; and in part by Toyota and Amazon. This article was presented in part at IEEE International Conference on Communications (ICC) 2025. *(Corresponding author: Jian Song.)*

Nan An and Fang Yang are with the Department of Electronic Engineering, Beijing National Research Center for Information Science and Technology, Tsinghua University, Beijing 100084, China (e-mail: an21@mails.tsinghua.edu.cn; fangyang@tsinghua.edu.cn).

Chang Liu is with the Center of National Railway Intelligent Transportation System Engineering and Technology and the Signal and Communication Research Institute, China Academy of Railway Sciences Corporation Ltd., Beijing 100081, China (e-mail: liuchangvista@163.com).

Ling Cheng is with the School of Electrical and Information Engineering, University of the Witwatersrand, Johannesburg 2050, South Africa (e-mail: ling.cheng@wits.ac.za).

Jian Song is with the Department of Electronic Engineering, Beijing National Research Center for Information Science and Technology, Tsinghua University, Beijing 100084, China, and also with the Shenzhen International Graduate School, Tsinghua University, Shenzhen 518055, China (e-mail: jsong@tsinghua.edu.cn).

Zhu Han is with the Department of Electrical and Computer Engineering, University of Houston, Houston, TX 77004 USA, and also with the Department of Computer Science and Engineering, Kyung Hee University, Seoul 446-701, South Korea (e-mail: hanzhu22@gmail.com).

Digital Object Identifier 10.1109/JIOT.2025.3534848

exists between the channel gain of edge and center vehicles, leading to unfairness among vehicles. Besides, vehicles at the cell edge experience intercell interference (ICI) from neighboring cells, which reduces their achievable data rates and further exacerbates unfairness among vehicles in multicell VLC systems [7].

To alleviate ICI, user-centric network design has been proposed for multicell VLC systems, where amorphous cells containing multiple APs are dynamically constructed and adjusted to facilitate collaborative information transmission to users within each cell [8], [9], [10], [11], [12], [13]. In [10], amorphous cells were formed through user-AP matching, with a proposed utility maximization algorithm enhancing user fairness. Similarly, AP-user pairs were built up according to the strength of channel gain in [11], followed by amorphous cell formation considering interuser distances to optimize average energy efficiency. Unlike the above works that treated cell construction and resource allocation separately, both tasks were completed together with the aim of maximizing energy efficiency [12]. Additionally, based on the constructed amorphous cells, the sum-rate maximization under the hybrid dimming constraint was investigated by optimizing the precoding matrix of APs in each cell [13]. Nevertheless, user-centric design requires the amount of APs to be no less than that of users [14], which is not suitable for vehicular VLC where the amount of streetlamps is less than that of vehicles. Furthermore, by leveraging a multidirection LED array, cooperation among multiple LEDs and the utilization of fractional frequency reuse effectively mitigated ICI [15], [16]. However, the multidirectional LED array required in this cooperative scheme does not match existing streetlamps, and cannot be directly utilized for vehicular VLC. In [17], employing three-color or four-color LEDs and orthogonal frequency division multiple access (OFDMA), a spatial signal-to-interference-plus-noise ratio (SINR) distribution as uniform as possible was obtained through the well-designed transmission configuration of frequency distribution, yet the allocation of power and other resources was not addressed.

Intelligent reflecting surface (IRS) is considered another approach to enhance fairness of the system because of its ability to actively modify the wireless channel by altering incident electromagnetic waves. In VLC, optical IRS (OIRS) is implemented by mirror arrays, metasurfaces, and liquid crystals, with the detailed properties of different designs discussed in [18], [19], and [20]. Motivated by cost-effectiveness, low-energy consumption, and flexible configuration, the application of OIRS has been widely studied [21], [22], with potential deployment in transmitters [23], receivers [24], and optical channels [25]. The deployment of OIRS in optical channels facilitates the construction of additional reflected links, thereby enhancing received signal strength and alleviating obstruction of the LoS link. In vehicular VLC, OIRS were deployed on the sides of vehicles [26] and streetlamp poles [27] to enhance both spectral and energy efficiencies in vehicle-to-vehicle (V2V) communications. In I2V communications from streetlamps to vehicles, OIRSs were deployed at the roadside to guarantee the requirements of bit error rate and achievable data rate [28]. However, existing research on OIRS application in vehicular VLC primarily focuses on the number of OIRS units needed to meet performance requirements, without addressing specific OIRS assignment schemes.

Inspired by the above work, a cooperative transmission approach is proposed for a multicell I2V vehicular VLC system with OIRS to improve fairness of the system. On the one hand, OIRS-reflected links enhance the channel gain of vehicles at the cell edge, thereby increasing their achievable data rates. In contrast to existing research on OIRS application in vehicular VLC, an OIRS assignment method is proposed for practical application that ensures max-min fairness in achievable data rates. On the other hand, cooperative transmission enables multiple VLC APs to allocate the same subchannels to a vehicle and transmit identical information simultaneously, converting potential ICI into useful signals and improving service quality. Unlike previous ICI alleviation methods, the proposed cooperative transmission is applicable when the number of streetlamps is less than the number of vehicles, and can be directly implemented with existing streetlamps without requiring specialized equipment, such as directional LED arrays. Moreover, the proposed method incorporates multidimensional resource allocation to further enhance max-min fairness among vehicles. Specifically, the main contributions of this article are as follows.

1) A cooperative transmission approach for a multicell vehicular VLC system with OIRS is proposed, and the corresponding system model is established in detail. By leveraging cooperative transmission and OIRS-reflected links, the achievable data rate of vehicles at the cell edge is improved, thereby enhancing max-min fairness of achievable data rates among vehicles.
2) Based on the proposed system model, a resource allocation problem is formulated to enhance max-min fairness by the joint allocation of OIRS, subchannels, and power. Furthermore, an effective resource allocation algorithm is proposed, in which the problem is initially reformulated into an equivalent form and then decomposed into three more tractable subproblems, which are solved iteratively by the block coordinate descent (BCD) algorithm. Within each BCD iteration, the subproblems of subchannel allocation, OIRS assignment, and power adjustment are addressed by the successive convex approximation (SCA) approach, the relaxation transformation (RT) scheme, and the minorization–maximization (MM) method, respectively.
3) The convergence and effectiveness of the proposed resource allocation algorithm are verified by numerical results. Compared with various baselines, the substantial improvement in max-min fairness resulting from both OIRS and the proposed cooperative transmission approach is also confirmed. In addition, the impact of key parameters, including the amount of OIRS units and the maximum power threshold, on the max-min fairness for the vehicular VLC system with OIRS is also revealed.

The remainder of this article is organized as follows. The system model and channel gain of the vehicular VLC system with OIRS are described in Section II. In Section III, the

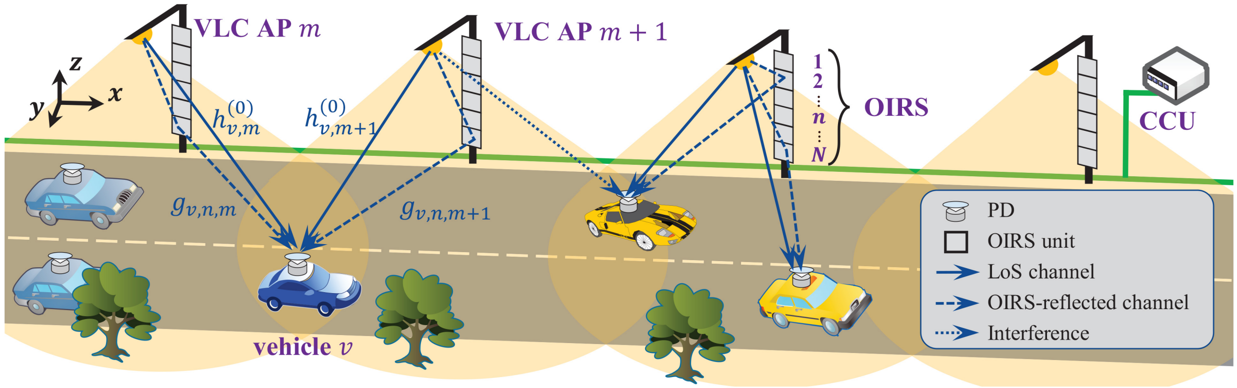

Fig. 1. System model of the OIRS-assisted vehicular VLC system with cooperative transmission.

max-min fairness enhancement problem is formulated, and the proposed BCD-based resource allocation algorithm is detailed in Section IV. Furthermore, numerical results are provided in Section V, and finally Section VI concludes this article.

Notation: Normal letters (e.g., x and X) and boldface letters (e.g., $\boldsymbol{x}$ and $\boldsymbol{X}$), and fancy capital letters (e.g., $\mathcal{X}$) denote scalars, vectors/matrices, and sets, respectively. Moreover, $(\cdot)^T$ and $\odot$ denote the transpose and Hadamard product of matrixes, respectively. Besides, the symbol of absolute value is presented by $|\cdot|$. The diagonal matrix is represented by $\text{diag}(x_1, x_2 \ldots, x_n)$, whose ith diagonal element of $x_i, i \in \{1, 2, \ldots, n\}$. In addition, $\boldsymbol{O}$, $\mathbf{0}_m$, and $\mathbf{1}_m$ represent the constant matrices and vectors of all-zero matrix, m-dimensional all-zero vector, and m-dimensional all-one vector, respectively. Furthermore, $\mathbb{R}$ and $\mathbb{B}$ demonstrate the fields of real numbers and binary numbers, respectively. Symbols of $\preceq$ and $\succeq$ denote that each element on the left-hand side is smaller or equal to and bigger than or equal to its counterpart on the right-hand side, respectively. $\arg\max(\cdot)$ is the arguments that make the following expression reach its maximum value.

II. System Model

As shown in Fig. 1, the illumination areas of multiple roadside streetlamps can cover all vehicles, providing the necessary infrastructure for I2V VLC [29], [30]. Specifically, streetlamps function as VLC APs for downlink communication, while each vehicle is equipped with a photodiode (PD) to receive optical signals. The index sets of VLC APs and vehicles are denoted by $\mathcal{M} = \{1, 2, \ldots, M\}$ and $\mathcal{V} = \{1, 2, \ldots, V\}$, respectively. Besides, all VLC APs are connected to the centralized control unit (CCU), which leverages its extensive computing capabilities to make resource allocation decisions [31], ensuring efficient fairness optimization. The CCU is typically located within a roadside unit (RSU) or at an edge computing node [32].

In the vehicular VLC system with OIRS, a vehicle receives signals from three types of channels, which are the LoS channels, the OIRS-reflected LoS channels, and non-LoS (NLoS) channels resulting from the diffuse reflection of surrounding objects. Due to the high location of streetlamps, the LoS links between VLC APs and PDs are easy to obtain without obstruction. Moreover, because of the weakness of the diffuse reflection, NLoS channel gain can be neglected [33]. Consequently, the characteristics of the LoS channel and OIRS-reflected channel are discussed in the following.

A. LoS Channel Gains

According to the Lambertian model [34], the LoS channel gain between VLC AP m and vehicle v is given by

$$h_{v,m}^{(0)} = \frac{(\kappa+1)q_v\Omega}{2\pi d_{v,m}^2}\cos^{\kappa}(\varphi_{v,m})\cos(\psi_{v,m})\Phi(\psi_{v,m}) \tag{1}$$

where κ, q_v, and Ω, represent the Lambertian index, the area of PD on vehicle v, and the optical filter gain, respectively. In addition, $d_{v,m}$, $\varphi_{v,m}$, and $\psi_{v,m}$ denote the distance between vehicle v and VLC AP m, the irradiance angle of the LED lamp on VLC AP m, and the incidence angle of the PD on vehicle v, respectively. Moreover, the optical concentrator gain is given by

$$\Phi(\psi_{v,m}) = \begin{cases} \frac{\chi^2}{\sin^2(\psi_0)}, & \text{if } 0 \le \psi_{v,m} \le \psi_0 \\ 0, & \text{otherwise} \end{cases} \tag{2}$$

where χ and ψ_0 represent the refractive index and the semi-angle of PD's field-of-view (FoV). Subsequently, the LoS channel gains between vehicle v and all VLC APs are denoted by $\boldsymbol{h}_v^{(0)} = [h_{v,1}^{(0)}, h_{v,2}^{(0)}, \ldots, h_{v,M}^{(0)}]^T$. Furthermore, the matrix of all LoS channel gains is given by $\boldsymbol{H}^{(0)} = [\boldsymbol{h}_1^{(0)}, \boldsymbol{h}_2^{(0)}, \ldots, \boldsymbol{h}_V^{(0)}]$.

B. OIRS-Reflected Channel Gains

With the aim of providing additional communication links, OIRSs with N units are installed on each lamppost, whose index set is demonstrated as $\mathcal{N} = \{1, 2, \ldots, N\}$. Existing lampposts can accommodate OIRS without requiring extra infrastructure and provide the necessary power supply to OIRS, thereby reducing deployment costs. Additionally, the height of the lampposts prevents the OIRS-reflected link from being obstructed. Furthermore, the OIRS units are arranged in a uniform linear array to match the shape of the lampposts. Considering the distance between streetlamps, OIRS on a lamppost is difficult to reflect the optical signals from other streetlamps, and only serves its corresponding streetlamp. In addition, through precise OIRS configuration, light reflection is fully controlled, preventing visual interference to the driver and ensuring compliance with regulatory requirements.

In view of the fact that the size of an OIRS unit is extremely larger than the wavelength of optical signals, the reflection of the OIRS unit is suitable to be analyzed by geometrical optics, especially the reflection law [35]. Moreover, since the size of LEDs is much smaller than the propagation distance of optical signals, the VLC AP can be regarded as a point light source [25]. Following the specular reflection, the optical signal can be viewed as emitted from a mirror light source symmetric to the LED about the OIRS unit, passing through the OIRS unit and arriving at the PD. Consequently, the specular reflection gain of the OIRS-reflected channel between VLC AP m to vehicle v reflected by unit n of the mth OIRS is given by [18] and [36]

$$g_{v,n,m} = \frac{\delta(\kappa+1)q_v\Omega\Phi\left(\hat{\psi}_{v,n}\right)}{2\pi\left(d^{(1)}_{n,m}+d^{(2)}_{v,n}\right)^2}\cos^{\kappa}\left(\hat{\varphi}_{n,m}\right)\cos\left(\hat{\psi}_{v,n}\right) \quad (3)$$

where δ denotes the reflectivity of the OIRS unit. Besides, $d^{(1)}_{n,m}$ and $d^{(2)}_{v,n}$ represent the distances between VLC AP m and OIRS unit n, and between vehicle v and OIRS unit n, respectively. Additionally, $\hat{\varphi}_{n,m}$ and $\hat{\psi}_{v,n}$ stand for the irradiance angle of the LED lamp on VLC AP m, and the incidence angle of the PD on vehicle v, respectively. Moreover, the OIRS-reflected channel gains between VLC AP m to vehicle v reflected by all OIRS units are denoted as $\boldsymbol{g}_{v,m} = [g_{v,1,m}, g_{v,2,m}, \ldots, g_{v,N,m}]^T$. Consequently, all OIRS-reflected channel gains of vehicle v are given by $\boldsymbol{G}_v = [\boldsymbol{g}_{v,1}, \boldsymbol{g}_{v,2}, \ldots, \boldsymbol{g}_{v,M}]$, which forms the set $\mathcal{G} = \{\boldsymbol{G}_v | v \in \mathcal{V}\}$.

As a vehicle moves, it periodically transmits its motion state information, such as location and speed, to the CCU through the uplink communication, thus CCU can predict the location of all vehicles in a resource allocation period [31]. Subsequently, based on the preknown locations of VLC APs and OIRSs, the roll and yaw angles of OIRS units can be calculated according to the reflection law if the OIRS unit is assigned to align with a VLC AP and a vehicle to construct a reflected link. As a result, the OIRS configuration problem is simplified to the assignment of the OIRS association relationship. To describe the unit assignment of the mth OIRS, binary variable $f_{m,n,v} = 1$ or 0 signifies the OIRS unit n of the mth OIRS is assigned to vehicle v or not. Furthermore, the unit assignment variables of the mth OIRS to vehicle v is denoted as $\boldsymbol{f}_{m,v} = [f_{m,1,v}, f_{m,2,v}, \ldots, f_{m,N,v}]^T$, which is the mth column of the matrix $\boldsymbol{F}_v = [\boldsymbol{f}_{1,v}, \boldsymbol{f}_{2,v}, \ldots, \boldsymbol{f}_{M,v}]$. Additionally, the assignment matrices of all OIRSs are included in a set $\mathcal{F} = \{\boldsymbol{F}_v | v \in \mathcal{V}\}$. Furthermore, the total OIRS-reflected channel gain from VLC AP m to vehicle v is $\boldsymbol{g}^T_{v,m}\boldsymbol{f}_{m,v}$, and the total OIRS-reflected channel gain from all VLC APs to vehicle v is given by

$$\boldsymbol{h}^{(1)}_v = \left[\boldsymbol{g}^T_{v,1}\boldsymbol{f}_{1,v}, \boldsymbol{g}^T_{v,2}\boldsymbol{f}_{2,v}, \ldots, \boldsymbol{g}^T_{v,M}\boldsymbol{f}_{M,v}\right]^T. \quad (4)$$

Considering both LoS channels and OIRS-reflected channels, the total channel gains from all VLC APs to vehicle v are demonstrated as

$$\boldsymbol{h}_v = \boldsymbol{h}^{(0)}_v + \boldsymbol{h}^{(1)}_v. \quad (5)$$

Moreover, the mth element of $\boldsymbol{h}_v$ is $h_{v,m}$, which is the total channel gains from VLC AP m to vehicle v.

III. Fairness Enhancement Problem Formulation

A. Subchannel Allocation and Power Adjustment

Because of the overlapping illumination areas of adjacent VLC APs, a vehicle may be within the service areas of multiple VLC APs. Hence, the association variable $s_{m,v}$ is formulated to represent the potential service relationships among all APs and vehicles, where $s_{m,v} = 1$ or 0 indicates that vehicle v can be served by VLC AP m or not. Therefore, the value of $s_{m,v}$ depends on the LoS channel gain between VLC AP m and vehicle v, which is given by

$$s_{m,v} = \begin{cases} 1, \ h^{(0)}_{v,m} > 0 \\ 0, \ h^{(0)}_{v,m} = 0. \end{cases} \quad (6)$$

Accordingly, the association matrix is defined as $\boldsymbol{S} \in \mathbb{B}^{M\times V}$, whose vth column is $\boldsymbol{s}_v = [s_{1,v}, s_{2,v}, \ldots, s_{M,v}]^T$.

Since a VLC AP affects all the vehicles within its coverage, OFDMA is employed so that a VLC AP can serve multiple vehicles simultaneously. With the bandwidth W of each subchannel, all subchannels are reused among all VLC APs, while the index set of all subchannels is given by $\mathcal{L} = \{1, 2, \ldots, L\}$. With the intention of describing the optical subchannel allocation, a variable $b_{m,v,l} = 1$ means that the subchannel l of VLC AP m is allocated to vehicle v, while 0 stands for nonallocation. For vehicle v, the allocation of the subchannel l of all VLC APs is denoted as $\boldsymbol{b}_{v,l} = [b_{1,v,l}, b_{2,v,l}, \ldots, b_{M,v,l}]^T$, which is the lth column of the matrix $\boldsymbol{B}_v = [\boldsymbol{b}_{v,1}, \boldsymbol{b}_{v,2}, \ldots, \boldsymbol{b}_{v,L}]$. Consequently, optical subchannel allocation matrices of all VLC APs form a set $\mathcal{B} = \{\boldsymbol{B}_v | v \in \mathcal{V}\}$. Furthermore, the optical subchannels of VLC AP m can be only allocated to the vehicles within its serving region, which means that $b_{m,v,l}$ can only be assigned a value of 1 when $s_{m,v} = 1$.

In the vehicular VLC system with OIRS, the power allocated to the subchannel l of VLC AP m is represented as $p_{m,l}$, which is the element in row m and column l of power matrix $\boldsymbol{P}$. Moreover, the power allocated to a subchannel of all VLC APs is denoted as $\boldsymbol{P}_l = \mathrm{diag}(p_{1,l}, p_{2,l}, \ldots, p_{M,l})$.

When a vehicle is located within the overlapping coverage of multiple VLC APs, optical signals from nonserving APs cause ICI, resulting in a reduced achievable data rate. The proposed cooperative transmission allows multiple VLC APs to allocate the same subchannels to the vehicle and transmit identical information upon them, while the transmitted signals are controlled by the CCU. In this case, potential ICI is converted into useful signals, thus alleviating ICI. As a result, the achievable data rate for vehicles at the cell edge is improved, ensuring fairness among vehicles. Moreover, jointly optimizing the OIRS assignment, subchannel allocation, and power adjustment in cooperative transmission effectively prioritizes resource allocation to vehicles experiencing disadvantaged reception conditions, thus improving fairness of the system.

B. Problem Formulation

As a result of the concentrated power density of the reflected optical beam, the energy leaked in directions other than the reflection direction of the OIRS is negligible [37]. Hence, if an OIRS unit is aligned with a VLC AP and a PD, its reflected optical signals do not interfere with other vehicles, demonstrating the no cross-talk property of OIRS [34]. Therefore, the ICI received by a vehicle only comes from the LoS channels from APs that do not serve this vehicle. Specifically, when the subchannel l of VLC AP m is not assigned to vehicle v, i.e., $b_{m,v,l} = 0$, the power allocated to the subchannel l of VLC AP m causes ICI to vehicle v through the LoS channel, which is given by $\sum_{m=1}^{M} (h_{v,m}^{(0)})^2 p_{m,l}(1 - b_{m,v,l})$. As a result, the SINR of vehicle v on subchannel l is given by

$$\gamma_{v,l} = \frac{\left(\boldsymbol{h}_v^T \boldsymbol{P}_l^{\frac{1}{2}} \boldsymbol{b}_{v,l}\right)^2}{\left(\boldsymbol{h}_v^{(0)} \odot \boldsymbol{h}_v^{(0)}\right)^T \boldsymbol{P}_l \left(\mathbf{1}_M - \boldsymbol{b}_{v,l}\right) + \sigma_{v,l}^2} \tag{7}$$

where $\sigma_{v,l}^2$ is the noise power on subchannel l received by vehicle v. Based on the proposed cooperative transmission of multiple VLC APs, the optical powers from the serving VLC APs are combined, as shown in the numerator of (7). Notably, whether a VLC AP participates in the cooperative transmission to vehicle v is not set in advance, but depends on the optimization result of the subchannel allocation. Subsequently, due to the different characteristics of RF and VLC, the Shannon capacity formula cannot be directly applied to VLC, so a lower bound on the achievable data rate of VLC [38], [39] is adopted to calculate the achievable data rate of vehicle v as

$$R_v = \sum_{l=1}^{L} \frac{W}{2} \log_2\left(1 + \frac{e}{2\pi}\gamma_{v,l}\right). \tag{8}$$

Selecting an appropriate fairness metric is essential to ensuring fairness among vehicles. Commonly used metrics include max-min fairness, proportional fairness, and Jain's index [40]. Max-min fairness focuses on maximizing the achievable data rate of the most disadvantaged vehicle, thus promoting equitable treatment [41]. In this case, the issue of extremely low-data rates for cell-edge vehicles is mitigated, which is particularly important for data-intensive applications, such as cooperative sensing, especially as vehicle movement may lead them into unfavorable reception conditions. In contrast, proportional fairness maximizes the sum of the logarithms of all vehicles' achievable data rates but often sacrifices the data rates of disadvantaged vehicles to improve the overall system performance, potentially resulting in significantly lower data rates for cell-edge vehicles [42]. Meanwhile, Jain's index emphasizes uniformity in achievable data rates across vehicles, which may result in uniformly low-data rates. Therefore, max-min fairness is chosen as the fairness metric for the I2V VLC system, and the corresponding optimization problem is formulated to maximize the minimum achievable data rate among all vehicles as

$$\text{(P0)} \quad \max_{\mathcal{F},\mathcal{B},\boldsymbol{P}} \min_{v} R_v \tag{9}$$

$$\text{s.t.} \quad \boldsymbol{P} \succeq \boldsymbol{O} \tag{9a}$$

$$\boldsymbol{P}\mathbf{1}_L \preceq \boldsymbol{p}_{\max} \tag{9b}$$

$$\mathbf{1}_M^T \boldsymbol{P}\mathbf{1}_L + Q \leq P_{\max} \tag{9c}$$

$$\boldsymbol{F}_v \in \mathbb{B}^{N\times M} \quad \forall\, v \in \mathcal{V} \tag{9d}$$

$$\sum_{v=1}^{V} f_{m,n,v} \leq 1 \quad \forall\, m \in \mathcal{M} \quad \forall\, n \in \mathcal{N} \tag{9e}$$

$$\boldsymbol{f}_{m,v}\left(1 - s_{m,v}\right) = \mathbf{0}_N \quad \forall\, m \in \mathcal{M}\ \forall\, v \in \mathcal{V} \tag{9f}$$

$$\boldsymbol{B}_v \in \mathbb{B}^{M\times L} \quad \forall\, v \in \mathcal{V} \tag{9g}$$

$$\sum_{v=1}^{V} b_{m,v,l} \leq 1 \quad \forall\, m \in \mathcal{M} \quad \forall\, l \in \mathcal{L} \tag{9h}$$

$$\boldsymbol{b}_{v,l} \odot (\mathbf{1}_M - \boldsymbol{s}_v) = \mathbf{0}_M \quad \forall\, v \in \mathcal{V} \quad \forall\, l \in \mathcal{L}. \tag{9i}$$

Constraints in the problem (P0) are explained as follows.

Power Adjustment Constraints: Constraint in (9a) ensures the nonnegative power allocation for the vehicular VLC system. To guarantee that the transmitted powers of all VLC APs are less than their maximum feasible powers $\boldsymbol{p}_{\max} = [p_{1,\max}, p_{2,\max}, \ldots, p_{M,\max}]^T$, constraint in (9b) is formulated. Besides, the total power consumption of the system less than the power threshold $P_{\max}$ is guaranteed by constraint in (9c), where $Q = MQ_1 + MNQ_2$ is the static power consumption of hardware. Specifically, Q_1 and Q_2 are hardware static power consumptions of a VLC AP and a unit of OIRS, respectively.

OIRS Assignment Constraints: The binary property of OIRS assignment variables is ensured by constraint in (9d). Due to the fact that an OIRS unit is assigned to at most one vehicle to construct a reflected channel, constraint in (9e) is established. Furthermore, constraint in (9f) ensures that each unit of an OIRS can only be assigned to vehicles within the serving region of the corresponding VLC AP. Specifically, the elements of $\boldsymbol{f}_{m,v}$ can be nonzero only if there is a potential service relationship between VLC AP m and vehicle v, i.e., $s_{m,v} = 1$.

Subchannel Allocation Constraints: Constraint in (9g) guarantees the binary property of subchannel allocation variables. Besides, constraint in (9h) means that any subchannel of a VLC AP is assigned to at most one vehicle. Moreover, similar to constraint in (9f), the restriction that each subchannel of VLC AP m can only be assigned to vehicles within its serving region is satisfied by constraint in (9i).

IV. Resource Allocation for Enhancing Fairness

On account of the difficulty in solving the problem (P0) in the max-min form, an auxiliary variable β is introduced to transform the problem (P0) into an equivalent problem as

$$\text{(P0-1)} \quad \max_{\mathcal{F},\mathcal{B},\boldsymbol{P},\beta} \beta \tag{10}$$

$$\text{s.t.} \quad \text{(9a)–(9i)}$$

$$R_v \geq \beta \quad \forall\, v \in \mathcal{V}. \tag{10a}$$

Subsequently, the solution of the problem (P0-1) satisfies

$$\beta = \min_{v} R_v \tag{11}$$

otherwise, the $\min_v R_v$ is a better solution, thus leading to a contradiction.

As both subchannel allocation and OIRS assignment are integer variables, and the achievable data rate exhibits nonlinearity, the problem (P0-1) is categorized as a mixed integer nonlinear programming (MINLP) problem. Owing to the nondeterministic polynomial (NP)-hard property of MINLP [43], the problem (P0-1) is intractable to be solved directly. Therefore, the problem (P0-1) is decomposed into three more solvable subproblems in this section, focusing on OIRS assignment, subchannel allocation, and power adjustment, which are solved by the SCA approach, RT scheme, and the MM method, respectively. Furthermore, all subproblems are solved iteratively according to the proposed BCD-based algorithm, in which a subproblem is solved while the other variables are fixed.

A. OIRS Assignment

With the given subchannel allocation $\mathcal{B}$ and power configuration $\boldsymbol{P}$, the assignment of OIRS is optimized, thereby the problem (P0-1) is transformed into

$$\begin{aligned} \text{(P1)}\quad & \max_{\mathcal{F},\beta} \beta \\ \text{s.t.}\quad & \text{(9d), (9e), (9f), (10a).} \end{aligned} \tag{12}$$

On account of the binary property of the OIRS assignment variables, the problem (P1) is an integer programming problem, which has been proven to be NP-hard [44]. While the optimal solution can be obtained through an exhaustive search within the feasible region, the computational complexity increases exponentially as the amount of optimization variables grows. Although the branch-and-bound method mitigates computational complexity by narrowing the search space, it still exhibits exponential complexity in the worst case scenario. In this section, an algorithm for OIRS assignment with low complexity is proposed, in which the discrete variables are relaxed to continuous variables and then reconstructed. Specifically, the discrete constraint in (9d) is relaxed to a continuous constraint as

$$\boldsymbol{O} \preceq \boldsymbol{F}_v \preceq \mathbf{1}_N \mathbf{1}_M^T \quad \forall\, v \in \mathcal{V}. \tag{13}$$

Based on the nonnegativity of elements in $\boldsymbol{F}_v$ and the sum constraint in (9e), it can be guaranteed that each element in $\boldsymbol{F}_v$ is less than 1. Subsequently, the relaxed constraint in (13) is further improved as

$$\boldsymbol{F}_v \succeq \boldsymbol{O} \quad \forall\, v \in \mathcal{V}. \tag{14}$$

Moreover, the nondecreasing property of R_v on $\boldsymbol{F}_v$ is given in Lemma 1.

Lemma 1: R_v is a nondecreasing function of each OIRS assignment variable $f_{m,n,v}$.

Proof: Considering the nonnegativity property of OIRS-reflected channel gains, as well as the linearity of (4) and (5), the total channel gain $h_{v,m}$ is a nondecreasing linear function with respect to $f_{m,n,v}$. Moreover, owing to the nonnegativity of $h_{v,m}$ and the quadratic form of $h_{v,m}$ in (7), $\gamma_{v,l}(h_{v,m})$ is an increasing function of $h_{v,m}$. Additionally, the achievable data rate R_v is an increasing function of $\gamma_{v,l}$ due to the logarithmic form in (8). According to the monotonicity of the compound function, R_v is a nondecreasing function of $f_{m,n,v}$. ■

As a result of constraint in (10a), the increase of R_v expands the feasible region of β, thereby leading to a larger β. To achieve this, on the basis of Lemma 1, the inequality constraint in (9e) is transformed into equality constraint as

$$\sum_{v=1}^{V} f_{m,n,v} = 1 \quad \forall\, m \in \mathcal{M} \quad \forall\, n \in \mathcal{N}. \tag{15}$$

Based on the above transformation, the OIRS assignment problem is rewritten as

$$\begin{aligned} \text{(P1-1)}\quad & \max_{\mathcal{F},\beta} \beta \\ \text{s.t.}\quad & \text{(9f), (10a), (14), (15).} \end{aligned} \tag{16}$$

On account of the nonconvex constraint in (10a), the problem (P1-1) is still hard to solve. In this case, a concave surrogate function is employed to locally approximate R_v, which approximates the feasible set of (10a) by a convex set from inside, thereby constructing an approximated subproblem. By constructing and solving a series of approximated subproblems, the optimization result converges to a stationary point of the original problem, which is the basic idea of the SCA algorithm [45]. To find a proper concave surrogate function, the first-order Taylor expansion is utilized as

$$\left(\boldsymbol{h}_v^T \boldsymbol{\xi}_{v,l}\right)^2 \geq \left(\hat{\boldsymbol{h}}_v^T \boldsymbol{\xi}_{v,l}\right)^2 + 2\hat{\boldsymbol{h}}_v^T \boldsymbol{\xi}_{v,l} \boldsymbol{\xi}_{v,l}^T \left(\boldsymbol{h}_v^{(1)} - \hat{\boldsymbol{h}}_v^{(1)}\right) \tag{17}$$

where $\hat{\boldsymbol{h}}_v$ and $\hat{\boldsymbol{h}}_v^{(1)}$ are obtained based on the OIRS assignment variables $\hat{\mathcal{F}}$ from last iteration, and $\boldsymbol{\xi}_{v,l} = \boldsymbol{P}_l^{1/2} \boldsymbol{b}_{v,l}$. Subsequently, the lower bound of SINR for vehicle v on subchannel l is given by

$$\underline{\gamma}_{v,l} = \frac{\left(\hat{\boldsymbol{h}}_v^T \boldsymbol{\xi}_{v,l}\right)^2 + 2\hat{\boldsymbol{h}}_v^T \boldsymbol{\xi}_{v,l} \boldsymbol{\xi}_{v,l}^T \left(\boldsymbol{h}_v^{(1)} - \hat{\boldsymbol{h}}_v^{(1)}\right)}{\left(\boldsymbol{h}_v^{(0)} \odot \boldsymbol{h}_v^{(0)}\right)^T \boldsymbol{P}_l \left(\mathbf{1}_M - \boldsymbol{b}_{v,l}\right) + \sigma_{v,l}^2}. \tag{18}$$

As a consequence, because of the monotonically increasing property of the logarithmic function, the surrogate lower bound of R_v is formulated and the approximated problem of the problem (P1-1) is expressed as

$$\begin{aligned} \text{(P1-2)}\quad & \max_{\mathcal{F},\beta} \beta \qquad\qquad (19)\\ \text{s.t.}\quad & \text{(9f), (14), (15)} \\ & \underline{R}_{1,v} = \sum_{l=1}^{L} \frac{W}{2} \log_2\left(1 + \frac{e}{2\pi} \underline{\gamma}_{v,l}\right) \geq \beta \quad \forall\, v \in \mathcal{V}. \qquad (19a) \end{aligned}$$

Similar to (11), the solution of the problem (P1-2) satisfies

$$\beta = \min_{v} \underline{R}_{1,v}(\boldsymbol{F}_v). \tag{20}$$

Moreover, to prove the convexity of the problem (P1-2), the concavity of $\underline{R}_{1,v}(\boldsymbol{F}_v)$ is discussed first.

Algorithm 1 SCA-Based OIRS Assignment Algorithm

Input: $\boldsymbol{S}, \boldsymbol{H}^{(0)}, \mathcal{G}, \mathcal{B}, \boldsymbol{P}$, and the error threshold $\varepsilon_1 > 0$.
Initialization: $\tau = 0$, $k = 1$, $\beta^{(0)}$ and $\mathcal{F}^{(0)}$ is initialized.
$\mathcal{F}^* = \mathcal{F}^{(0)}$, $R^* = \min_v R_v(\mathcal{F}^{(0)})$;
repeat
  Construct the lower bound $\underline{R}_{1,v}(\boldsymbol{F}_v)$ based on $\mathcal{F}^{(\tau)}$;
  Solve the problem (P1-2) by IPM and obtain $\beta^{(\tau+1)}$, $\mathcal{F}^{(\tau+1)}$;
  $\tau = \tau + 1$;
until $|\min_v R_v(\mathcal{F}^{(\tau)}) - \min_v R_v(\mathcal{F}^{(\tau-1)})| < \varepsilon_1$
$\overline{\mathcal{F}} = \mathcal{F}^{(\tau)}$;
repeat
  Generate $\tilde{\boldsymbol{F}}^{(k)}$ and reconstruct $\check{\mathcal{F}}^{(k)}$ based on (22);
  if $R^* < \min_v R_v(\check{\mathcal{F}}^{(k)})$ **then**
    $\mathcal{F}^* = \check{\mathcal{F}}^{(k)}$, $R^* = \min_v R_v(\check{\mathcal{F}}^{(k)})$;
  end if
  $k = k + 1$;
until $k > K$
Output: $\mathcal{F}^*$

Proposition 1: For $\forall\, v \in \mathcal{V}$, $\underline{R}_{1,v}(\boldsymbol{F}_v)$ is a concave function.

Proof: According to (18), $\underline{\gamma}_{v,l}$ is a affine function of $\boldsymbol{F}_v$. Since the log function is concave and nondecreasing, the compound function of the log function and $\underline{\gamma}_{v,l}$ is concave [46]. Furthermore, $\underline{R}_{1,v}(\boldsymbol{F}_v)$ is the sum of multiple compound concave functions and is therefore concave. ■

Based on Proposition 1, constraint in (19a) is a convex constraint. Considering the affine objective function and affine constraints in (9f), (14), and (15), the problem (P1-2) is a convex optimization problem, which is then solved by the interior point method (IPM), thus obtaining the continuous OIRS assignment results $\overline{\mathcal{F}}$. For the purpose of reconstructing the binary OIRS assignment, a uniform randomization method is proposed. To this end, the elements accumulation of $\overline{\mathcal{F}}$ is first defined as

$$\Upsilon_{m,n}(v) = \begin{cases} \sum_{\hat{v}=1}^{v} \bar{f}_{m,n,\hat{v}}, & \forall\, v \in \mathcal{V} \\ 0, & v = 0. \end{cases} \tag{21}$$

Specifically, a random matrix $\tilde{\boldsymbol{F}} \in \mathbb{R}^{M\times N}$ is generated, whose element $\tilde{f}_{m,n}$ obeys uniform distribution from 0 to 1. Then, a construction of $\mathcal{F}$ is given by

$$\check{f}_{m,n,v} = \begin{cases} 1, & \Upsilon_{m,n}(v-1) \le \tilde{f}_{m,n} \le \Upsilon_{m,n}(v) \\ 0, & \text{otherwise.} \end{cases} \tag{22}$$

The above generation of $\tilde{\boldsymbol{F}}$ and reconstruction of $\mathcal{F}$ are repeated K times, thus obtaining K reconstructed OIRS assignment variables. The reconstruction result that maximizes the max-min fairness is selected as the final OIRS assignment. To sum up, the above SCA-based OIRS assignment algorithm is illustrated in Algorithm 1.

B. Subchannel Allocation

Focusing on the subchannel allocation problem, the problem (P0-1) with the given OIRS assignment $\mathcal{F}$ and power configuration $\boldsymbol{P}$ is transformed into

$$\begin{aligned} \text{(P2)} \quad & \max_{\mathcal{B},\beta} \beta \\ & \text{s.t.} \quad \text{(9g), (9h), (9i), (10a).} \end{aligned} \tag{23}$$

In virtue of the binary constraint in (9g), the subchannel allocation problem is also an integer programming. Similar to the OIRS assignment problem, the discrete variables are relaxed first and reconstructed after optimization. Specifically, the binary constraint in (9g) is relaxed to

$$\boldsymbol{O} \preceq \boldsymbol{B}_v \preceq \mathbf{1}_M \mathbf{1}_L^T \quad \forall\, v \in \mathcal{V} \tag{24}$$

where the nonnegativity of elements in $\boldsymbol{B}_v$ is guaranteed. Furthermore, due to constraint in (9h), which ensures that the sum of elements is less than 1, each element in $\boldsymbol{B}_v$ is guaranteed to be less than 1. As a result, constraint in (24) is simplified as

$$\boldsymbol{B}_v \succeq \boldsymbol{O} \quad \forall\, v \in \mathcal{V}. \tag{25}$$

Besides, the following auxiliary variables are introduced to transform the problem (P2) into a more tractable form as:

$$\theta_{m,v,l} = \sqrt{p_{m,l}}\left(1 - b_{m,v,l}\right) \quad \forall\, m \in \mathcal{M} \quad \forall\, v \in \mathcal{V} \quad \forall\, l \in \mathcal{L}. \tag{26}$$

Furthermore, the vector of $\theta_{m,v,l}$ is demonstrated as $\boldsymbol{\theta}_{v,l} = [\theta_{1,v,l}, \theta_{2,v,l}, \ldots, \theta_{M,v,l}]^T$, which is the lth column of $\boldsymbol{\Theta}_v = [\boldsymbol{\theta}_{v,1}, \boldsymbol{\theta}_{v,2}, \ldots, \boldsymbol{\theta}_{v,L}]$, and the set of all auxiliary variables is formulate as $\vartheta = \{\boldsymbol{\Theta}_v | v \in \mathcal{V}\}$. Subsequently, the inverse transformation is given by

$$b_{m,v,l} = \begin{cases} 1 - \frac{\theta_{m,v,l}}{\sqrt{p_{m,l}}}, & p_{m,l} > 0 \\ 0, & p_{m,l} = 0. \end{cases} \tag{27}$$

If the power allocated to subchannel l of VLC AP m is 0, whether this subchannel is allocated or not has no impact on the objective function, and thus it is assumed that this subchannel is not allocated to any vehicle. Accordingly, constraints in (9h), (9i), and (25) are transformed to

$$\sum_{v=1}^{V} \theta_{m,v,l} \ge \sqrt{p_{m,l}}(V-1) \quad \forall\, m \in \mathcal{M} \quad \forall\, l \in \mathcal{L} \tag{28}$$

$$\left(\boldsymbol{P}_l^{\frac{1}{2}} \mathbf{1}_L - \boldsymbol{\theta}_{v,l}\right) \odot (\mathbf{1}_M - \boldsymbol{s}_v) = \mathbf{0}_M \quad \forall\, v \in \mathcal{V} \quad \forall\, l \in \mathcal{L} \tag{29}$$

$$\boldsymbol{\theta}_{v,l} \preceq \boldsymbol{P}_l^{\frac{1}{2}} \mathbf{1}_L \quad \forall\, v \in \mathcal{V} \quad \forall\, l \in \mathcal{L}. \tag{30}$$

As a result of the above variable transformation, the problem (P2) is relaxed to

$$\begin{aligned} \text{(P2-1)} \quad & \max_{\vartheta,\beta} \beta \\ & \text{s.t.} \quad \text{(10a), (28), (29), (30).} \end{aligned} \tag{31}$$

In an attempt to deal with the difficulty brought by the nonconvex constraint in (10a), the approximated subproblem is constructed by replacing (10a) with its global lower bound, thereby the solution sequence converges to the Karush–Kuhn–Tucker (KKT) point [47] of the problem (P2-1). To find a global lower bound of (10a), the following lemma is introduced.

Lemma 2: The inequality $\log_2(1+\eta) \geq \rho \log_2(\eta)+\omega$ holds for any nonnegative η and η_0 with coefficients of

$$\rho = \frac{\eta_0}{1+\eta_0} \tag{32}$$

$$\omega = \log_2(1+\eta_0) - \rho \log_2 \eta_0. \tag{33}$$

When $\eta = \eta_0$, the expressions on both sides of the inequality are equal, as are their first-order derivatives [48].

As a consequence, a lower bound of R_v is formulated as

$$\underline{R}_{2,v}(\boldsymbol{\Theta}_v) = \sum_{l=1}^{L} \frac{W}{2}\left[D_{v,l}\left(\boldsymbol{\theta}_{v,l}\right) - J_{v,l}\left(\boldsymbol{\theta}_{v,l}\right)\right] \tag{34}$$

where the terms involving ϑ are represented by

$$D_{v,l}\left(\boldsymbol{\theta}_{v,l}\right) = 2\rho_{v,l} \log_2\left(\sqrt{\frac{e}{2\pi}}\boldsymbol{h}_v^T\left(\boldsymbol{P}_l^{\frac{1}{2}}\mathbf{1}_L - \boldsymbol{\theta}_{v,l}\right)\right) + \omega_{v,l} \tag{35}$$

$$J_{v,l}\left(\boldsymbol{\theta}_{v,l}\right) = \rho_{v,l} \log_2\left((\boldsymbol{h}_v^{(0)} \odot \boldsymbol{h}_v^{(0)})^T \boldsymbol{P}_l^{\frac{1}{2}} \boldsymbol{\theta}_{v,l} + \sigma_{v,l}^2\right). \tag{36}$$

Coefficients $\rho_{v,l}^{(\tau)}$ and $\omega_{v,l}^{(\tau)}$ of the τth iteration are calculated according to (32) and (33) with

$$\eta_0^{(\tau)} = \frac{e}{2\pi}\gamma_{v,l}^{(\tau)}. \tag{37}$$

Furthermore, on the basis of the first-order Taylor expansion of the logarithmic function that

$$\log_2(\alpha) \leq \log_2(\alpha_0) + \frac{\alpha - \alpha_0}{\alpha_0 \ln(2)} \tag{38}$$

the upper bound of (36) is obtained as

$$J_{v,l}^{(1)}\left(\boldsymbol{\theta}_{v,l}\right) = J_{v,l}\left(\hat{\boldsymbol{\theta}}_{v,l}\right) + \frac{\rho_{v,l}}{\ln(2)} \cdot \frac{\left(\boldsymbol{h}_v^{(0)} \odot \boldsymbol{h}_v^{(0)}\right)^T \boldsymbol{P}_l^{\frac{1}{2}}\left(\boldsymbol{\theta}_{v,l} - \hat{\boldsymbol{\theta}}_{v,l}\right)}{\left(\boldsymbol{h}_v^{(0)} \odot \boldsymbol{h}_v^{(0)}\right)^T \boldsymbol{P}_l^{\frac{1}{2}}\hat{\boldsymbol{\theta}}_{v,l} + \sigma_{v,l}^2} \tag{39}$$

where $\hat{\boldsymbol{\theta}}_{v,l}$ is the optimization result of last iteration. Accordingly, the lower bound of R_v is further improved and the approximated problem of the problem (P2-1) is then constructed as

$$\text{(P2-2)} \quad \max_{\vartheta,\beta} \beta \tag{40}$$

$$\text{s.t.} \quad (28), (29), (30)$$

$$\hat{\underline{R}}_{2,v} = \sum_{l=1}^{L} \frac{W}{2}\left[D_{v,l}\left(\boldsymbol{\theta}_{v,l}\right) - J_{v,l}^{(1)}\left(\boldsymbol{\theta}_{v,l}\right)\right] \geq \beta \quad \forall\, v \in \mathcal{V}. \tag{40a}$$

To prove the convexity of the problem (P2-2), the concavity of $\hat{\underline{R}}_{2,v}(\boldsymbol{\Theta}_v)$ is discussed first.

Proposition 2: For $\forall\, v \in \mathcal{V}$, $\hat{\underline{R}}_{2,v}(\boldsymbol{\Theta}_v)$ is a concave function.

Proof: The logarithmic function is both nondecreasing and concave, and $D_{v,l}(\boldsymbol{\theta}_{v,l})$ is a composition of the logarithmic function and an affine function. Therefore, based on the properties of composition functions [46], $D_{v,l}(\boldsymbol{\theta}_{v,l})$ is concave with respect to $\boldsymbol{\theta}_{v,l}$. Besides, it is obvious that $J_{v,l}^{(1)}(\boldsymbol{\theta}_{v,l})$ is an affine function with respect to $\boldsymbol{\theta}_{v,l}$. As a result, $\hat{\underline{R}}_{2,v}(\boldsymbol{\Theta}_v)$ is the sum of multiple concave and affine functions on l, rendering it concave. ∎

Algorithm 2 RT-Based Subchannel Allocation Algorithm

Input: $\boldsymbol{S}, \boldsymbol{H}^{(0)}, \mathcal{G}, \mathcal{F}, \boldsymbol{P}$, and the error threshold $\varepsilon_2 > 0$
Initialization: $\tau = 0$, $\beta^{(0)}$ and $\mathcal{B}^{(0)}$ is initialized.
Transform $\mathcal{B}^{(0)}$ to $\vartheta^{(0)}$ according to (26);
repeat
  Calculate $\gamma_{v,l}^{(\tau)}$ based on $\vartheta^{(\tau)}$ for $\forall\, v \in \mathcal{V}$, $\forall\, l \in \mathcal{L}$;
  Calculate $\rho_{v,l}^{(\tau)}$ and $\omega_{v,l}^{(\tau)}$ for $\forall\, v \in \mathcal{V}$, $\forall\, l \in \mathcal{L}$ according to (32) and (33);
  Construct $\hat{\underline{R}}_{2,v}(\boldsymbol{\Theta}_v)$ based on $\vartheta^{(\tau)}$, $\rho_{v,l}^{(\tau)}$ and $\omega_{v,l}^{(\tau)}$;
  Solve the problem (P2-2) by IPM and obtain $\beta^{(\tau+1)}$, $\vartheta^{(\tau+1)}$;
  $\tau = \tau + 1$;
until $|\min_v R_v(\mathcal{B}^{(\tau)}) - \min_v R_v(\mathcal{B}^{(\tau-1)})| < \varepsilon_2$
$\vartheta^* = \vartheta^{(\tau)}$, $m = 1$, $l = 1$;
Convert ϑ^* to $\mathcal{B}^*$ according to (27);
repeat
  repeat
    $v^* = \arg\max_v b_{m,v,l}^*$;
    $b_{m,v^*,l}^* = 1$ and $b_{m,v\neq v^*,l}^* = 0$;
    $l = l + 1$;
  until $l > L$
  $m = m + 1$, $l = 1$;
until $m > M$
Output: $\mathcal{B}^*$

In accordance with Proposition 2, constraint in (40a) is a convex constraint. In addition, the objective function and other constraints are affine, so the problem (P2-2) is convex, which can be solved by convex optimization algorithms. In the follow-up phase of obtaining the continuous optimization result ϑ^*, it is inverse transformed to $\mathcal{B}^*$. Consequently, the binary subchannel allocation is reconstructed by allocating the subchannel l of VLC AP m to the vehicle v^* with the largest $b_{m,v,l}^*$ among all vehicles, whereupon all constraints of the problem (P2) are satisfied. To sum up, details about the proposed RT-based subchannel allocation algorithm are shown in Algorithm 2.

C. Power Adjustment

In this section, the powers allocated to all subchannels are optimized with the given OIRS assignment $\mathcal{F}$ and subchannel allocation $\mathcal{B}$. Consequently, the problem (P0-1) is transformed into

$$\text{(P3)} \quad \max_{\boldsymbol{P},\beta} \beta$$

$$\text{s.t.} \quad (9a), (9b), (9c), (10a). \tag{41}$$

For the sake of convenience, a variable transformation is introduced as

$$c_{m,l} = \sqrt{p_{m,l}} \quad \forall\, m \in \mathcal{M} \quad \forall\, l \in \mathcal{L} \tag{42}$$

which is the element in row m and column l of matrix $\boldsymbol{C}$. Besides, the variables after transformation are defined as $\boldsymbol{C}_l = \text{diag}(c_{1,l}, c_{2,l}, \ldots, c_{M,l})$. Accordingly, constraints in (9a), (9b), and (9c) are transformed to

$$\boldsymbol{C} \succeq \boldsymbol{O} \tag{43}$$

$$(\boldsymbol{C} \odot \boldsymbol{C})\mathbf{1}_L \preceq \boldsymbol{p}_{\max} \tag{44}$$

$$\mathbf{1}_M^T(\boldsymbol{C} \odot \boldsymbol{C})\mathbf{1}_L + Q \leq P_{\max}. \tag{45}$$

In conformity with the transformation in (26) and (42), $D_{v,l}$ and $J_{v,l}$ are also demonstrated as

$$D_{v,l}(\boldsymbol{C}_l) = 2\rho_{v,l}\log_2\left(\sqrt{\frac{e}{2\pi}}\boldsymbol{h}_v^T\boldsymbol{C}_l\boldsymbol{b}_{v,l}\right) + \omega_{v,l} \tag{46}$$

$$J_{v,l}(\boldsymbol{C}_l) = \rho_{v,l}\log_2\left((\boldsymbol{h}_v^{(0)} \odot \boldsymbol{h}_v^{(0)})^T\boldsymbol{C}_l^2(\mathbf{1}_M - \boldsymbol{b}_{v,l}) + \sigma_{v,l}^2\right). \tag{47}$$

In accordance with inequality (38), the upper bound of $J_{v,l}(\boldsymbol{C}_l)$ is represented as

$$J_{v,l}^{(2)}(\boldsymbol{C}_l) = J_{v,l}\left(\hat{\boldsymbol{C}}_l\right) + \frac{\rho_{v,l}\left(\boldsymbol{h}_v^{(0)} \odot \boldsymbol{h}_v^{(0)}\right)^T\left(\boldsymbol{C}_l^2 - \hat{\boldsymbol{C}}_l^2\right)\left(\mathbf{1}_M - \boldsymbol{b}_{v,l}\right)}{\ln(2)\left((\boldsymbol{h}_v^{(0)} \odot \boldsymbol{h}_v^{(0)})^T\hat{\boldsymbol{C}}_l^2(\mathbf{1}_M - \boldsymbol{b}_{v,l}) + \sigma_{v,l}^2\right)} \tag{48}$$

where $\hat{\boldsymbol{C}}_l$ is the optimization result of last iteration. Subsequently, the lower bound of R_v with respect to $\boldsymbol{C}_l$ is formulated and the approximated problem constructed by MM method for the power adjustment problem is illustrated as

$$\text{(P3-1)} \quad \max_{\boldsymbol{P},\beta} \beta \tag{49}$$

$$\text{s.t.} \quad (43), (44), (45)$$

$$\underline{R}_{3,v} = \sum_{l=1}^{L}\frac{W}{2}\left[D_{v,l}(\boldsymbol{C}_l) - J_{v,l}^{(2)}(\boldsymbol{C}_l)\right] \geq \beta \ \ \forall\, v \in \mathcal{V}. \tag{49a}$$

To prove the convexity of the problem (P3-1), the concavity of $\underline{R}_{3,v}(\boldsymbol{C})$ is discussed first.

Proposition 3: For $\forall\, v \in \mathcal{V}$, $\underline{R}_{3,v}(\boldsymbol{C})$ is a concave function.

Proof: Due to the concavity of the affine function and the logarithmic function, as well as the nondecreasing property of the logarithmic function, $D_{v,l}(\boldsymbol{C}_l)$ is a concave function with respect to $\boldsymbol{C}_l$ according to the concave-convex properties of compound functions [46]. On the other hand, $J_{v,l}^{(2)}(\boldsymbol{C}_l)$ is a quadratic function with positive coefficients of quadratic terms and hence convex. Therefore, $\underline{R}_{3,v}(\boldsymbol{C})$ is a concave function since it is the sum of $D_{v,l}(\boldsymbol{C}_l)$ and $-J_{v,l}^{(2)}(\boldsymbol{C}_l)$ on l. ■

The objective function of the problem (P3-1) and constraint in (43) are affine functions of optimization variables, which are also convex. Additionally, constraints in (44) and (45) are quadratic constraints with positive coefficients, thus they are convex constraints. On the basis of Proposition 3, constraint in (49a) is also a convex constraint. Consequently, the problem (P3-1) is a convex optimization problem, which is solved by the convex optimization algorithms, followed by the inverse transformation from optimization results $\boldsymbol{C}^*$ to $\boldsymbol{P}^*$. In summary, the MM-based power adjustment algorithm is represented in Algorithm 3.

D. BCD-Based Algorithm for Fairness Optimization

Based on the above algorithms focusing on OIRS assignment, subchannel allocation, and power adjustment, three subproblems are solved iteratively until the gap of the max-min fairness during two consecutive iterations is less than the threshold, as shown in Algorithm 4.

Algorithm 3 MM-Based Power Adjustment Algorithm

Input: $\boldsymbol{S}, \boldsymbol{H}^{(0)}, \mathcal{G}, \mathcal{F}, \mathcal{B}$, and the error threshold $\varepsilon_3 > 0$
Initialization: $\tau = 0$, $\beta^{(0)}$ and $\boldsymbol{P}^{(0)}$ is initialized.
Convert $\boldsymbol{P}^{(0)}$ to $\boldsymbol{C}^{(0)}$ according to (42);
repeat
  Calculate $\gamma_{v,l}^{(\tau)}$ based on $\boldsymbol{C}^{(\tau)}$ for $\forall\, v \in \mathcal{V},\ \forall\, l \in \mathcal{L}$;
  Calculate $\rho_{v,l}^{(\tau)}$ and $\omega_{v,l}^{(\tau)}$ for $\forall\, v \in \mathcal{V},\ \forall\, l \in \mathcal{L}$ according to (32) and (33);
  Construct $\underline{R}_{3,v}(\boldsymbol{\Theta}_v)$ based on $\boldsymbol{C}^{(\tau)}$, $\rho_{v,l}^{(\tau)}$ and $\omega_{v,l}^{(\tau)}$;
  Solve the problem (P3-1) by IPM and obtain $\beta^{(\tau+1)}$, $\boldsymbol{C}^{(\tau+1)}$;
  $\tau = \tau + 1$;
until $|\min_v R_v(\boldsymbol{C}^{(\tau)}) - \min_v R_v(\boldsymbol{C}^{(\tau-1)})| < \varepsilon_3$
$\boldsymbol{C}^* = \boldsymbol{C}^{(\tau)}$;
Convert $\boldsymbol{C}^*$ inversely to $\boldsymbol{P}^*$ according to (42);
Output: $\boldsymbol{P}^*$

For the purpose of analyzing the convergence of the proposed BCD-based resource allocation algorithm, the convergences of algorithms for three subproblems are first discussed. In the τth iteration of Algorithm 1, the max-min fairness does not decrease, which is guaranteed by

$$\min_v R_v\left(\boldsymbol{F}_v^{(\tau-1)}\right) \overset{a}{=} \min_v \underline{R}_{1,v}\left(\boldsymbol{F}_v^{(\tau-1)}\right) \overset{b}{=} \beta^{(\tau-1)} \overset{c}{\leq} \beta^{(\tau)} \overset{d}{=} \min_v \underline{R}_{1,v}\left(\boldsymbol{F}_v^{(\tau)}\right) \overset{e}{\leq} \min_v R_v\left(\boldsymbol{F}_v^{(\tau)}\right). \tag{50}$$

Equation (50a) holds because $\boldsymbol{F}_v^{(\tau-1)}$ is the Taylor expansion point of (17) in the τth loop. Besides, (50b) and (50d) are ensured by the property in (20). In addition, the validity of inequality (50c) is guaranteed by the execution of IPM, while the inequality (50e) holds because $\underline{R}_{1,v}$ is a lower bound of R_v. Furthermore, to avoid possible reduction of the max-min fairness caused by the reconstruction of binary OIRS assignment variables, the results of Algorithm 1 are selected from the reconstructed variables and those obtained in the previous iteration, which is given by

$$\mathcal{F}^{(i)} = \arg\max_{\mathcal{F}}\left(\min_v R_v(\mathcal{F}^{(i-1)}), \min_v R_v(\mathcal{F}^*)\right). \tag{51}$$

Accordingly, the nondecreasing property $\min_v R_v(\mathcal{F}^{(i)}) \geq \min_v R_v(\mathcal{F}^{(i-1)})$ holds in the ith iteration of Algorithm 4.

Similar to the analysis of (50), the nondecreasing property for subchannel allocation and power adjustment in the τth loop of Algorithms 2 and 3 can also be formulated, respectively. Additionally, the selection procedure of subchannel allocation variables is demonstrated as

$$\mathcal{B}^{(i)} = \arg\max_{\mathcal{B}}\left(\min_v R_v(\mathcal{B}^{(i-1)}), \min_v R_v(\mathcal{B}^*)\right). \tag{52}$$

As a consequence, the nondecreasing property of the Step 6 and Step 7 in Algorithm 4 holds, which is given by $\min_v R_v(\mathcal{B}^{(i)}) \geq \min_v R_v(\mathcal{B}^{(i-1)})$ and $\min_v R_v(\boldsymbol{P}^{(i)}) \geq \min_v R_v(\boldsymbol{P}^{(i-1)})$ in the ith iteration, respectively.

Algorithm 4 BCD-Based Resource Allocation Algorithm

1: **Input**: $\boldsymbol{S}$, $\boldsymbol{H}^{(0)}$, $\mathcal{G}$, and the error threshold $\varepsilon_4 > 0$.
2: **Initialization**: $i = 0$, $\mathcal{F}^{(0)}$, $\mathcal{B}^{(0)}$, and $\boldsymbol{P}^{(0)}$ are given.
3: **repeat**
4: $i = i + 1$;
5: With given $\mathcal{B}^{(i-1)}$ and $\boldsymbol{P}^{(i-1)}$, solve OIRS assignment problem by **Algorithm 1** and obtain $\mathcal{F}^{(i)}$;
6: With given $\mathcal{F}^{(i)}$ and $\boldsymbol{P}^{(i-1)}$, solve subchannel allocation problem by **Algorithm 2** and obtain $\mathcal{B}^{(i)}$;
7: With given $\mathcal{F}^{(i)}$ and $\mathcal{B}^{(i)}$, solve power adjustment problem by **Algorithm 3** and obtain $\boldsymbol{P}^{(i)}$;
8: **until** $|\min_v R_v^{(i)} - \min_v R_v^{(i-1)}| < \varepsilon_4$
9: **Output**: $\mathcal{B}^{(i)}$, $\mathcal{F}^{(i)}$ and $\boldsymbol{P}^{(i)}$.

Taking the above discussions into account, the max-min fairness does not decrease during the iteration of the proposed BCD-based algorithm, which is formulated as

$$\min_v R_v\left(\mathcal{B}^{(i-1)}, \mathcal{F}^{(i-1)}, \boldsymbol{P}^{(i-1)}\right) \le \min_v R_v\left(\mathcal{B}^{(i)}, \mathcal{F}^{(i)}, \boldsymbol{P}^{(i)}\right).$$

Moreover, because of the finite feasible region of the problem (P0), the max-min fairness is upper-bounded by a finite value, leading to its convergence as the iterations proceed. However, since the objective function is not jointly concave with respect to optimization variables, the solution provided by the proposed BCD-based fairness enhancement algorithm is suboptimal.

E. Computational Complexity Analysis

In Algorithm 1 for OIRS assignment, the problem (P1-2) is solved by IPM with the complexity of $\mathcal{O}((MNV+1)^{3.5}\log_2(1/\hat{\varepsilon}_1))$, where $\hat{\varepsilon}_1$ is the solution accuracy. Additionally, the computational complexity of OIRS assignment reconstruction is $\mathcal{O}(MNL(V+\log_2(V)))$. Considering that the iteration number of Algorithm 1 is $\mathcal{O}(\log_2(1/\varepsilon_1))$, the overall complexity of Algorithm 1 is $r_1 = \mathcal{O}(((MNV+1)^{3.5}\log_2(1/\hat{\varepsilon}_1) + MNL(V+\log_2(V)))\log_2(1/\varepsilon_1))$. Based on the similar analyses, the computational complexity of Algorithms 2 and 3 are $r_2 = \mathcal{O}(((MVL+1)^{3.5}\log_2(1/\hat{\varepsilon}_2) + MVL)\log_2(1/\varepsilon_2))$ and $r_3 = \mathcal{O}(((ML+1)^{3.5}\log_2(1/\hat{\varepsilon}_3))\log_2(1/\varepsilon_3))$, respectively, where $\hat{\varepsilon}_2$ and $\hat{\varepsilon}_3$ are the solution accuracy in corresponding algorithms. In summary, for the proposed BCD-based resource allocation algorithm in Algorithm 4, the iteration number is $\mathcal{O}(\log_2(1/\varepsilon_4))$, and hence the overall computational complexity of Algorithm 4 is $\mathcal{O}((r_1+r_2+r_3)\log_2(1/\varepsilon_4))$.

V. Simulation Results

In this section, comprehensive simulations are conducted to evaluate the effectiveness of the proposed BCD-based resource allocation algorithm for max-min fairness enhancement of the OIRS-assisted vehicular VLC system with cooperative transmission. Moreover, the simulation parameters are listed in Table I, which remain unchanged in this section unless otherwise stated. As for the simulation scenario, different VLC APs have the same y-coordinate and z-coordinate, which are

TABLE I
Simulation Parameters

Parameter	Value
Number of VLC APs, M	5
Number of OIRS units, N	40
Number of vehicles, V	13
Number of subchannels, L	40
Bandwidth of each subchannel, W	5 MHz
Lambertian index, κ	1
Optical filter gain, Ω	1
Semi-angle of PD's FOV, ψ_0	70°
Refractive index of a PD, χ	1.5
Area of PD, q_v	1 cm^2
Reflectivity of OIRS units, δ	0.9
Size of OIRS units	5 cm
Noise power, $\sigma_{v,l}^2$	5×10^{-16} W
Maximum power of each VLC AP, $p_{m,\max}$	4 W
Static power consumption of a VLC AP, Q_1	1 W
Static power consumption of an OIRS unit, Q_2	0.01 W
Power threshold $P_{\max}$	20 W
Number of uniform randomization, K	500

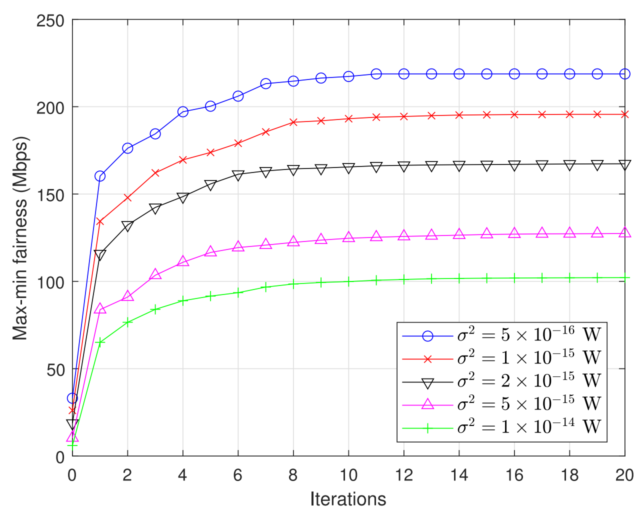

Fig. 2. Convergence of the proposed BCD-based resource allocation algorithm under different noise powers.

0.97 m and 8.26 m, respectively, and their x-coordinates are 10 m, 30 m, 50 m, 70 m, and 90 m, respectively. For each OIRS, the x-coordinate is the same as that of the corresponding VLC AP, while the y-coordinate and z-coordinate of its midpoint are 0 and 4.5 m, respectively. In addition, the size of each vehicle is 4 m × 2.2 m, and the height of the PD on each vehicle is 1 m. Besides, vehicles are randomly distributed on a two-lane road, with each lane having a width of 3.5 m. For ease of expression, the max-min fairness in achievable data rates is denoted by $R_{\min}$ in the following, which stands for the max-min fairness of the I2V VLC system.

A. Simulation of the BCD-Based Algorithm

The convergence of the proposed BCD-based resource allocation algorithm under varying noise powers is depicted in Fig. 2. As the number of iterations increases, $R_{\min}$ keeps

Fig. 3. Resource allocation results of the proposed BCD-based algorithm. (a) OIRS assignment. (b) Subchannel allocation. (c) Power adjustment (mW).

increasing and converges within 8 iterations, confirming the convergence analysis in Section IV-D. In addition, the proposed BCD-based algorithm significantly improves max-min fairness through iterations compared to the initial iteration point, with more pronounced improvements observed as the noise power decreases. With a noise power of 5×10^{-16} W, the proposed algorithm improves $R_{\min}$ by over 180 Mb/s after several iterations, validating its effectiveness.

When the proposed algorithm converges with a noise power of 5×10^{-16} W, the resource allocation results are illustrated in Fig. 3, with Fig. 3(a) and (b) showing the allocation of OIRS units and subchannels of VLC APs to specific vehicles, respectively, while Fig. 3(c) presents the power allocation for each subchannel. The resource allocation results reveal that when a vehicle is located in the overlapping coverage area of adjacent cells, both VLC APs can allocate the same subchannel to the vehicle for cooperative transmission, effectively reducing ICI. Furthermore, OIRS units in both cells are assigned to this vehicle to establish OIRS-reflected links, thereby enhancing its channel gain thus improving its achievable data rate, as shown by vehicles 3, 4, 7, and 9. In terms of power adjustment, the proposed algorithm tends to allocate more power to subchannels utilized by cell-edge vehicles with low-channel gains, such as vehicle 3. These results demonstrate that the proposed algorithm effectively mitigates the disadvantages faced by cell-edge vehicles, ensuring max-min fairness of the I2V VLC system.

The performance of the proposed algorithm in maintaining max-min fairness during vehicle movement is illustrated in Fig. 4. In the simulation, vehicles moving at 10 m/s along the road serve as an example to demonstrate the impact of vehicle movement on max-min fairness, while the proposed algorithm is still applicable in scenarios with other typical speeds. In this context, the change in relative position between vehicles and streetlamps is characterized by the movement time. Throughout the time interval depicted in Fig. 4, each

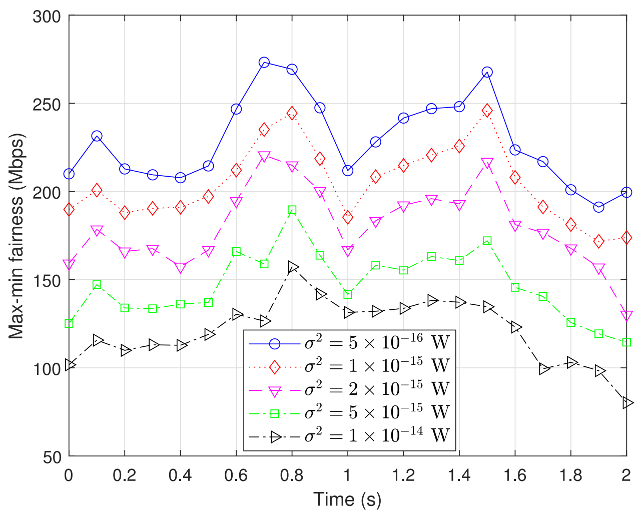

Fig. 4. Variation of the max-min fairness $R_{\min}$ among vehicles with respect to time.

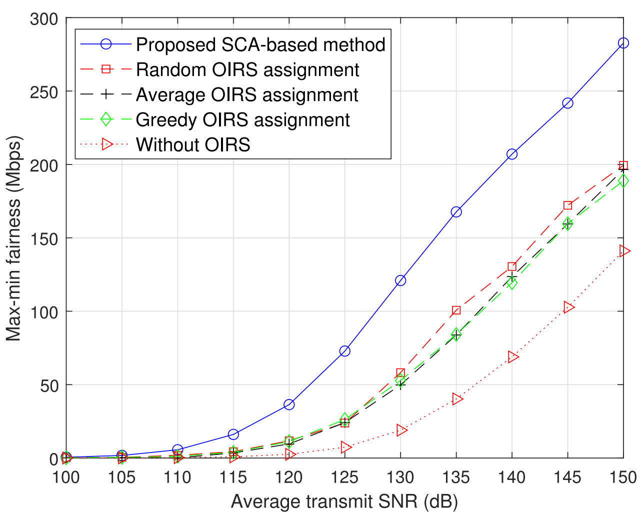

Fig. 5. Max-min fairness $R_{\min}$ among vehicles versus the average transmit SNR with different OIRS assignment methods.

vehicle transitions from one cell to another. As vehicles move, their changing relative positions to the streetlamps alter the channel gains, leading to fluctuations in max-min fairness of the system. Moreover, under different noise conditions, effectively meets the data rate requirements of disadvantaged vehicles, further demonstrating the algorithm's effectiveness in ensuring max-min fairness during vehicle movement.

B. Comparison With Multiple Baselines

The proposed methods for solving three subproblems are compared with other benchmarks about OIRS assignment, subchannel allocation, and power adjustment under different average transmit signal-to-noise ratios (SNRs), which are calculated by

$$\mathrm{SNR}_{\mathrm{ave}} = 10\log_{10}\left(\frac{\mathbf{1}_M^T \boldsymbol{P} \mathbf{1}_L}{ML\sigma_{v,l}^2}\right). \tag{53}$$

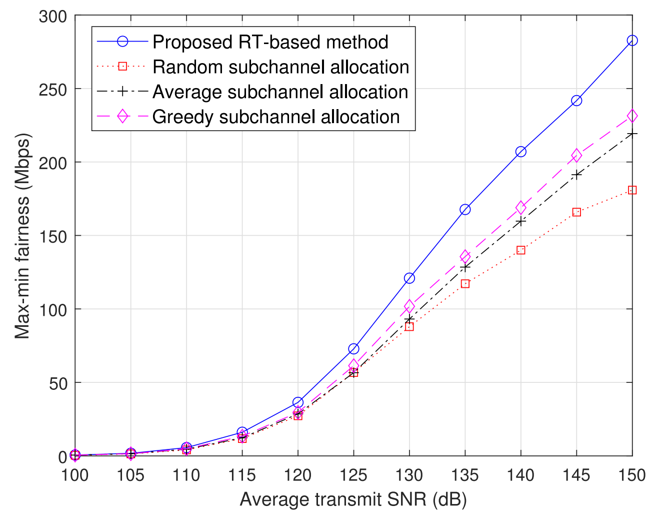

Fig. 6. Max-min fairness $R_{\min}$ among vehicles versus the average transmit SNR with different subchannel allocation methods.

In Fig. 5, the proposed SCA-based OIRS assignment method is compared with the following benchmarks, while the methods for subchannel allocation and power adjustment remain the same.

1) *Random OIRS Assignment:* Assign OIRS units to vehicles in the serving region randomly.
2) *Average OIRS Assignment:* The amount of OIRS units assigned to each vehicle is as equal as possible.
3) *Greedy OIRS Assignment:* OIRS units are assigned one by one to the vehicle with the lowest current achievable data rate in its service region.
4) *Without OIRS:* No OIRS is utilized.

As shown in Fig. 5, $R_{\min}$ increases with the rise in average transmit SNR for all methods. In the low-SNR region, the performance of the proposed SCA-based OIRS assignment method closely resembles that of baselines, as both struggle to achieve high $R_{\min}$ due to noise influence. Conversely, the SCA-based algorithm notably outperforms baselines as the average transmit SNR grows. Specifically, at an average transmit SNR of 150 dB, the SCA-based algorithm exhibits over a 140 Mb/s improvement compared with the case without OIRS and an 86 Mb/s improvement compared with the other three baselines. Compared with the case without OIRS, the improvement in max-min fairness results from OIRS enhancing the received signal strength through the additional reflective links, thereby elevating $R_{\min}$ significantly. Furthermore, since LoS channel gains for vehicles at a VLC cell center are stronger than those for vehicles at a VLC cell edge, more OIRS units are allocated to vehicles at a VLC cell edge to enhance their achievable data rate, thereby ensuring max-min fairness. However, average and random allocation methods fail to meet this requirement, resulting in lower max-min fairness compared with the SCA-based algorithm.

For subchannel allocation, the proposed RT-based scheme is compared with the following baselines to demonstrate its effectiveness, while maintaining the same OIRS assignment and power adjustment methods.

1) *Random Subchannel Allocation:* Subchannels of an AP are allocated to vehicles in its serving region randomly.

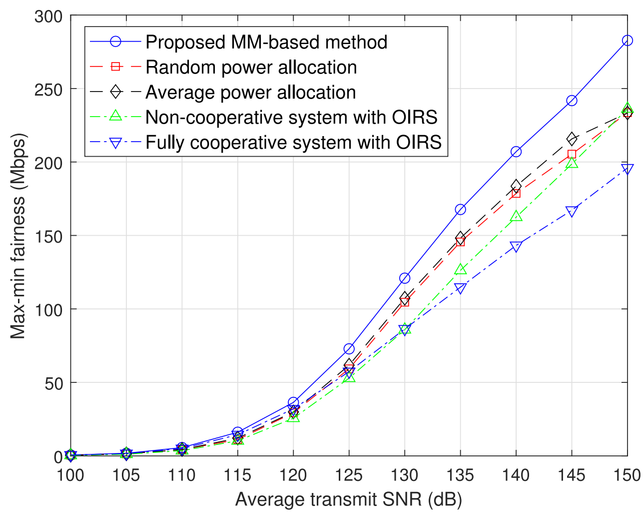

Fig. 7. Max-min fairness $R_{\min}$ among vehicles versus the average transmit SNR with different power adjustment methods and various cooperative strategies.

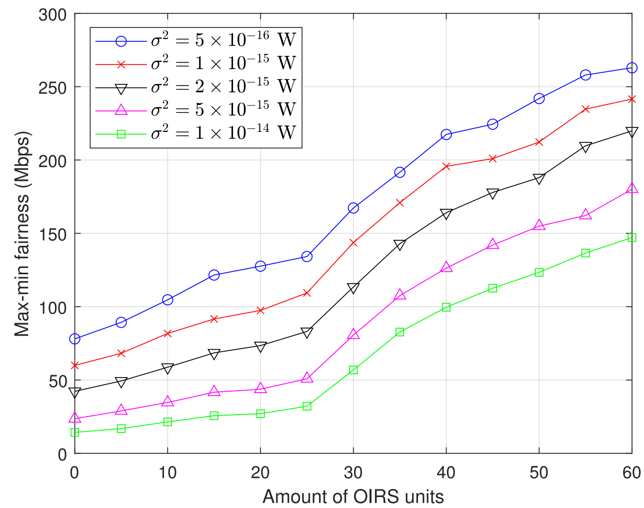

Fig. 8. Max-min fairness $R_{\min}$ among vehicles versus the amount of OIRS units N.

2) *Average Subchannel Allocation:* The number of subchannels assigned to each vehicle is as equal as possible.
3) *Greedy Subchannel Allocation:* Subchannels are allocated one by one to the vehicle with the lowest current achievable data rate in its service region.

As demonstrated in Fig. 6, the proposed RT-based scheme outperforms other baselines at any SNR regions. For vehicles located at a VLC cell edge, optical signals from multiple VLC APs lead to ICI. However, with the help of cooperative transmission, the ICI is mitigated when multiple APs transmit identical information over the same subchannel to a vehicle. Furthermore, through comprehensively optimizing the assignment of all subchannels, max-min fairness is effectively enhanced. On the contrary, random allocation struggles to allocate identical subchannels of different APs to the same vehicle, hampering interference mitigation and consequently limiting the potential enhancement of $R_{\min}$. In the case of average allocation, vehicles with both strong and weak channel gains are equally treated, thereby hindering effective fairness enhancement. Besides, for greedy allocation, the possible ICI is overlooked when subchannels are assigned one by one, resulting in lower max-min fairness compared with the RT-based scheme.

In Fig. 7, the proposed MM-based power adjustment is compared with the following baselines with the same total power consumption, while the OIRS assignment and subchannel allocation methods remain the same.

1) *Random Power Allocation:* Power is randomly allocated to subchannels of all VLC APs.
2) *Uniform Power Allocation:* For all subchannels of all VLC APs, the power is uniformly allocated.

Both random and uniform power allocation methods neglect the difference in channel gain among vehicles and potential ICI, resulting in ineffective enhancement of achievable data rates for disadvantaged vehicles. In contrast, these factors are taken into consideration by the MM-based algorithm, thereby enhancing max-min fairness. Specifically, at an average transmit SNR of 150 dB, the MM-based algorithm exhibits over a 30% improvement in $R_{\min}$ compared with the other two benchmarks.

The advantage of the proposed cooperative transmission approach is further illustrated by comparing it with the OIRS-assisted noncooperative VLC system and the OIRS-assisted fully cooperative VLC system in Fig. 7.

1) *Noncooperative System:* Each vehicle is served by only one VLC AP, treating optical signals from other VLC APs as interference, with no cooperative transmission allowed.
2) *Fully Cooperative System:* If a vehicle is within the serving regions of multiple VLC APs, it is served by them simultaneously, where the ICI is avoided.

As observed from the simulation in Fig. 7, the proposed cooperative transmission system with the proposed BCD-based algorithm demonstrates superior max-min fairness compared with both the noncooperative and fully cooperative systems. For the noncooperative system, the ICI caused by multiple VLC APs is not alleviated, leading to inadequate achievable data rate improvements for disadvantaged vehicles. Additionally, while the fully cooperative system mitigates potential ICI, it suffers from inefficient resource utilization. Particularly, when a vehicle is within the service area of multiple VLC APs, the same subchannels of these APs are allocated to the vehicle to mitigate the ICI. However, if the vehicle's channel gain from a particular VLC AP is weak, its contribution to signal enhancement is very limited. In contrast, reallocating the subchannel of the VLC AP with weak channel gain to other vehicles effectively improves their achievable data rates with limited ICI to the current vehicle, and hence the fully cooperative system struggles to improve max-min fairness. Compared with these systems, ICI is alleviated by cooperative transmission with the proposed BCD-based algorithm, effectively enhancing max-min fairness while making full use of communication resources.

C. Influence of Key Parameters

The impact of the amount of OIRS units N on max-min fairness across various noise powers is depicted in Fig. 8, in

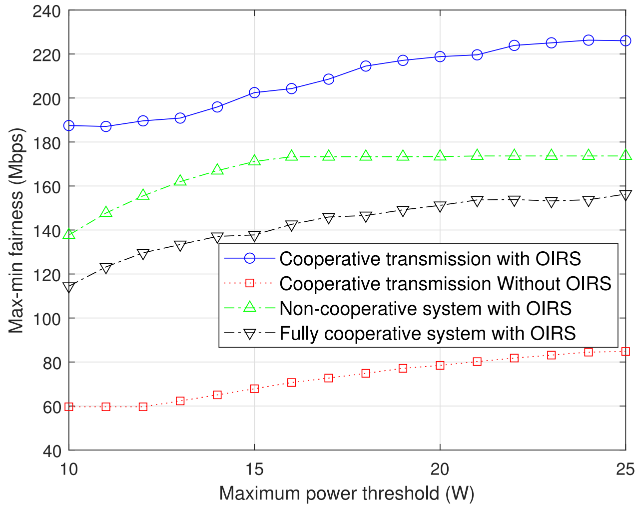

Fig. 9. Max-min fairness $R_{\min}$ among vehicles versus the maximum power threshold $P_{\max}$.

which $R_{\min}$ gradually increases as N grows. To be specific, at a noise power of 5×10^{-16} W, employing OIRSs with 40 units results in an improvement in $R_{\min}$ of over 130 Mb/s compared with scenarios without OIRS. In the low-noise power situation, max-min fairness experiences a significant increase as N increases. This phenomenon arises because the achievable data rate of vehicles is primarily determined by the strength of the received signal and interference, both of which are effectively managed by the proposed BCD-based algorithm. Conversely, under a high-noise power condition, the achievable data rate of vehicles is primarily influenced by the received signal power and noise power. Thus, while increasing N enhances the received signal strength through the construction of additional reflective links, the resulting improvement in achievable data rate is less pronounced compared with low-noise power scenarios.

In Fig. 9, the variation of max-min fairness in various systems with the maximum power threshold $P_{\max}$ is demonstrated. With the increase of $P_{\max}$, $R_{\min}$ of each system gradually rises as more power becomes available for disadvantaged vehicles, thereby enhancing their achievable data rates. Moreover, for the cooperative transmission system, utilizing OIRS results in a substantial improvement in $R_{\min}$ of over 120 Mb/s compared with the case without OIRS, which validates the advantage of OIRS in constructing additional communication links through reflection and enhancing the received signal strength. In addition, while the noncooperative system disregards the influence of ICI entirely and the fully cooperative system avoids it completely, the proposed cooperative transmission strikes a balance between the two extremes. By enhancing the received SINR through interference elimination while reducing the waste of resources, the proposed cooperative transmission system achieves higher max-min fairness compared with other baselines.

VI. Conclusion

In this article, a cooperative transmission approach for a multicell vehicular VLC system with OIRS is proposed to improve max-min fairness among vehicles, with the construction of a detailed system model. Consequently, the resource allocation problem is then formulated and transformed into an equivalent form, which is then decomposed into three subproblems, and iteratively solved by the BCD algorithm. Specifically, the subproblems of OIRS assignment, subchannel allocation, and power adjustment are addressed by SCA, RT, and MM algorithms, respectively. Furthermore, simulation results demonstrate that the proposed BCD-based resource allocation algorithm yields significant improvements in max-min fairness of achievable data rates compared with other baselines. In addition, compared with the vehicular VLC system with noncooperative transmission and with fully cooperative transmission, the proposed cooperative transmission approach effectively enhances max-min fairness, confirming its potential to alleviate ICI and fully utilize resources. Moreover, as the amount of OIRS units and maximum power threshold grows, the max-min fairness also rises, significantly outperforming vehicular VLC systems without cooperative transmission or without OIRS. In future work, the proposed BCD-based algorithm would be extended to resource allocation problems aimed at achieving proportional fairness and sum data rate maximization. Furthermore, the multiobjective resource allocation problem would be explored to take into account the tradeoffs among various performance metrics of I2V VLC systems. Besides, the potential applications of VLC in V2V communications would be explored, offering new solutions for communication systems in ITS.

References

[1] N. An, F. Yang, C. Liu, L. Cheng, J. Song, and Z. Han, "Max-min fairness enhancement in OIRS-assisted I2V cooperative VLC system for robotaxis," in *Proc. IEEE Int. Conf. Commun. (ICC) Workshop*, 2025, to be published.

[2] T. Zhou, C. Li, W. Zhang, B. Ai, L. Liu, and Y. Liang, "Narrowbeam channel measurements and characterization in vehicle-to-infrastructure scenarios for 5G-V2X communications," *IEEE Internet Things J.*, vol. 11, no. 9, pp. 16074–16086, May 2024.

[3] G. Sun et al., "Geometric-based channel modeling and analysis for double-RIS-aided vehicle-to-vehicle communication systems," *IEEE Internet Things J.*, vol. 11, no. 10, pp. 18888–18901, May 2024.

[4] H. Zhang et al., "Mean-field-aided multiagent reinforcement learning for resource allocation in vehicular networks," *IEEE Internet Things J.*, vol. 10, no. 3, pp. 2667–2679, Feb. 2023.

[5] A.-M. Cailean and M. Dimian, "Current challenges for visible light communications usage in vehicle applications: A survey," *IEEE Commun. Surveys Tuts.*, vol. 19, no. 4, pp. 2681–2703, 4th Quart., 2017.

[6] A. Memedi and F. Dressler, "Vehicular visible light communications: A survey," *IEEE Commun. Surveys Tuts.*, vol. 23, no. 1, pp. 161–181, 1st Quart., 2021.

[7] H. Zhang, N. Liu, K. Long, J. Cheng, V. C. M. Leung, and L. Hanzo, "Energy efficient subchannel and power allocation for software-defined heterogeneous VLC and RF networks," *IEEE J. Sel. Areas Commun.*, vol. 36, no. 3, pp. 658–670, Mar. 2018.

[8] X. Li, R. Zhang, and L. Hanzo, "Optimization of visible-light optical wireless systems: Network-centric versus user-centric designs," *IEEE Commun. Surveys Tuts.*, vol. 20, no. 3, pp. 1878–1904, 3rd Quart., 2018.

[9] R. Zhang, J. Wang, Z. Wang, Z. Xu, C. Zhao, and L. Hanzo, "Visible light communications in heterogeneous networks: Paving the way for user-centric design," *IEEE Wireless Commun.*, vol. 22, no. 2, pp. 8–16, Apr. 2015.

[10] X. Li, F. Jin, R. Zhang, J. Wang, Z. Xu, and L. Hanzo, "Users first: User-centric cluster formation for interference-mitigation in visible-light networks," *IEEE Trans. Wireless Commun.*, vol. 15, no. 1, pp. 39–53, Jan. 2016.

[11] R. Zhang, H. Claussen, H. Haas, and L. Hanzo, "Energy efficient visible light communications relying on amorphous cells," *IEEE J. Sel. Areas Commun.*, vol. 34, no. 4, pp. 894–906, Apr. 2016.
[12] M. Obeed, A. M. Salhab, S. A. Zummo, and M.-S. Alouini, "New algorithms for energy-efficient VLC networks with user-centric cell formation," *IEEE Trans. Green Commun. Netw.*, vol. 3, no. 1, pp. 108–121, Mar. 2019.
[13] Y. Yang et al., "Joint LED selection and precoding optimization for multiple-user multiple-cell VLC systems," *IEEE Internet Things J.*, vol. 9, no. 8, pp. 6003–6017, Apr. 2022.
[14] M. Obeed, A. M. Salhab, M.-S. Alouini, and S. A. Zummo, "On optimizing VLC networks for downlink multi-user transmission: A survey," *IEEE Commun. Surveys Tuts.*, vol. 21, no. 3, pp. 2947–2976, 3rd Quart., 2019.
[15] S. Aboagye, T. M. N. Ngatched, O. A. Dobre, and A. G. Armada, "Energy efficient subchannel and power allocation in cooperative VLC systems," *IEEE Commun. Lett.*, vol. 25, no. 6, pp. 1935–1939, Jun. 2021.
[16] S. Aboagye, T. M. N. Ngatched, and O. A. Dobre, "Subchannel and power allocation in downlink VLC under different system configurations," *IEEE Trans. Wireless Commun.*, vol. 21, no. 5, pp. 3179–3191, May 2022.
[17] B. G. Guzmán, A. A. Dowhuszko, V. P. G. Jiménez, and A. I. Pérez-Neira, "Resource allocation for cooperative transmission in optical wireless cellular networks with illumination requirements," *IEEE Trans. Commun.*, vol. 68, no. 10, pp. 6440–6455, Oct. 2020.
[18] A. M. Abdelhady, O. Amin, A. K. S. Salem, M.-S. Alouini, and B. Shihada, "Channel characterization of IRS-based visible light communication systems," *IEEE Trans. Commun.*, vol. 70, no. 3, pp. 1913–1926, Mar. 2022.
[19] A. R. Ndjiongue, T. M. N. Ngatched, O. A. Dobre, and H. Haas, "Re-configurable intelligent surface-based VLC receivers using tunable liquid-crystals: The concept," *J. Lightw. Technol.*, vol. 39, no. 10, pp. 3193–3200, May 15, 2021.
[20] S. Aboagye, A. R. Ndjiongue, T. M. N. Ngatched, and O. A. Dobre, "Design and optimization of liquid crystal RIS-based visible light communication receivers," *IEEE Photon. J.*, vol. 14, no. 6, pp. 1–7, Dec. 2022.
[21] S. Aboagye, A. R. Ndjiongue, T. M. N. Ngatched, O. A. Dobre, and H. V. Poor, "RIS-assisted visible light communication systems: A tutorial," *IEEE Commun. Surveys Tuts.*, vol. 25, no. 1, pp. 251–288, 1st Quart., 2023.
[22] H. Wang, Z. Zhang, B. Zhu, J. Dang, and L. Wu, "Optical reconfigurable intelligent surfaces aided optical wireless communications: Opportunities, challenges, and trends," *IEEE Wireless Commun.*, vol. 30, no. 5, pp. 28–35, Oct. 2023.
[23] S. Aboagye, T. M. N. Ngatched, A. R. Ndjiongue, O. A. Dobre, and H. Shin, "Liquid crystal-based RIS for VLC transmitters: Performance analysis, challenges, and opportunities," *IEEE Wireless Commun.*, vol. 31, no. 4, pp. 98–105, Aug. 2024.
[24] O. Maraqa and T. M. N. Ngatched, "Optimized design of joint mirror array and liquid crystal-based RIS-aided VLC systems," *IEEE Photon. J.*, vol. 15, no. 4, pp. 1–11, Aug. 2023.
[25] S. Sun, T. Wang, F. Yang, J. Song, and Z. Han, "Intelligent reflecting surface-aided visible light communications: Potentials and challenges," *IEEE Veh. Technol. Mag.*, vol. 17, no. 1, pp. 47–56, Mar. 2022.
[26] P. Sharda, "Next generation based vehicular visible light communications: A novel transmission scheme," *IEEE Trans. Veh. Technol.*, vol. 73, no. 11, pp. 16735–16743, Nov. 2024.
[27] H. B. Eldeeb, S. Naser, L. Bariah, and S. Muhaidat, "Energy and spectral efficiency analysis for RIS-aided V2V-visible light communication," *IEEE Commun. Lett.*, vol. 27, no. 9, pp. 2373–2377, Sep. 2023.
[28] H. B. Eldeeb, M. Qaraqe, S. Muhaidat, and A. Ghrayeb, "Reconfigurable intelligent surfaces-assisted I2V-visible light communication," in *Proc. IEEE Int. Mediterr. Conf. Commun. Netw. (MeditCom)*, Jul. 2024, pp. 465–470.
[29] H. B. Eldeeb, M. Elamassie, S. M. Sait, and M. Uysal, "Infrastructure-to-vehicle visible light communications: Channel modelling and performance analysis," *IEEE Trans. Veh. Technol.*, vol. 71, no. 3, pp. 2240–2250, Mar. 2022.
[30] M. S. Demir, H. B. Eldeeb, and M. Uysal, "CoMP-based dynamic handover for vehicular VLC networks," *IEEE Commun. Lett.*, vol. 24, no. 9, pp. 2024–2028, Sep. 2020.
[31] J. Chen, Z. Wang, and T. Mao, "Resource management for hybrid RF/VLC V2I wireless communication system," *IEEE Commun. Lett.*, vol. 24, no. 4, pp. 868–871, Apr. 2020.
[32] W. Feng, S. Lin, N. Zhang, G. Wang, B. Ai, and L. Cai, "Joint C-V2X based offloading and resource allocation in multi-tier vehicular edge computing system," *IEEE J. Sel. Areas Commun.*, vol. 41, no. 2, pp. 432–445, Feb. 2023.
[33] K. Ying, H. Qian, R. J. Baxley, and S. Yao, "Joint optimization of precoder and Equalizer in MIMO VLC systems," *IEEE J. Sel. Areas Commun.*, vol. 33, no. 9, pp. 1949–1958, Sep. 2015.
[34] S. Sun, N. An, F. Yang, J. Song, and Z. Han, "Capacity Characterization analysis of optical intelligent reflecting surface assisted MISO VLC," *IEEE Internet Things J.*, vol. 11, no. 3, pp. 4801–4814, Feb. 2024.
[35] V. Jamali, H. Ajam, M. Najafi, B. Schmauss, R. Schober, and H. V. Poor, "Intelligent reflecting surface assisted free-space optical communications," *IEEE Commun. Mag.*, vol. 59, no. 10, pp. 57–63, Oct. 2021.
[36] A. M. Abdelhady, A. K. S. Salem, O. Amin, B. Shihada, and M.-S. Alouini, "Visible light communications via intelligent reflecting surfaces: Metasurfaces vs mirror arrays," *IEEE Open J. Commun. Soc.*, vol. 2, pp. 1–20, 2021.
[37] S. Sun, W. Mei, F. Yang, N. An, J. Song, and R. Zhang, "Optical intelligent reflecting surface assisted MIMO VLC: Channel modeling and capacity characterization," *IEEE Trans. Wireless Commun.*, vol. 23, no. 3, pp. 2125–2139, Mar. 2024.
[38] A. Lapidoth, S. M. Moser, and M. A. Wigger, "On the capacity of free-space optical intensity channels," *IEEE Trans. Inf. Theory*, vol. 55, no. 10, pp. 4449–4461, Oct. 2009.
[39] S. Aboagye, T. M. N. Ngatched, O. A. Dobre, and H. V. Poor, "Energy-efficient resource allocation for aggregated RF/VLC systems," *IEEE Trans. Wireless Commun.*, vol. 22, no. 10, pp. 6624–6640, Oct. 2023.
[40] H. Shi, R. V. Prasad, E. Onur, and I. G. M. M. Niemegeers, "Fairness in wireless networks: Issues, measures and challenges," *IEEE Commun. Surveys Tuts.*, vol. 16, no. 1, pp. 5–24, 1st Quart., 2014.
[41] Y. Shen, C. Wang, W. Zang, L. Xue, B. Yang, and X. Guan, "Outage constrained max–min secrecy rate optimization for IRS-aided SWIPT systems with artificial noise," *IEEE Internet Things J.*, vol. 11, no. 6, pp. 9814–9828, Mar. 2024.
[42] A. A. Khan and R. S. Adve, "Percentile optimization in wireless networks—Part-I: Power control for max-min-rate to sum-rate maximization (and everything in between)," *IEEE Trans. Signal Process.*, vol. 72, pp. 1518–1532, 2024.
[43] A. Alizadeh and M. Vu, "Load balancing user association in millimeter wave MIMO networks," *IEEE Trans. Wireless Commun.*, vol. 18, no. 6, pp. 2932–2945, Jun. 2019.
[44] M. Bohge, J. Gross, A. Wolisz, and M. Meyer, "Dynamic resource allocation in OFDM systems: An overview of cross-layer optimization principles and techniques," *IEEE Netw.*, vol. 21, no. 1, pp. 53–59, Jan./Feb. 2007.
[45] G. Scutari, F. Facchinei, and L. Lampariello, "Parallel and distributed methods for constrained nonconvex optimization—Part-I: Theory," *IEEE Trans. Signal Process.*, vol. 65, no. 8, pp. 1929–1944, Apr. 2017.
[46] S. Boyd and L. Vandenberghe, *Convex Optimization*. Cambridge, U.K.: Cambridge Univ. Press, 2004.
[47] Y. Sun, P. Babu, and D. P. Palomar, "Majorization-minimization algorithms in signal processing, communications, and machine learning," *IEEE Trans. Signal Process.*, vol. 65, no. 3, pp. 794–816, Feb. 2017.
[48] J. Papandriopoulos and J. S. Evans, "Low-complexity distributed algorithms for spectrum balancing in multi-user DSL networks," in *Proc. IEEE Int. Conf. Commun.*, vol. 7, Istanbul, Türkey, Jun. 2006, pp. 3270–3275.

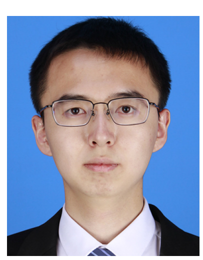

Nan An received the B.S. degree from the Department of Electronic Engineering, Tsinghua University, Beijing, China, in 2021, where he is currently pursuing the Ph.D. degree with the DTV Technology Research and Development Center, Department of Electronic Engineering.

His research interests are in the field of visible light communications, integrated control and communication, and vehicular communications.

Fang Yang (Senior Member, IEEE) received the B.S.E. and Ph.D. degrees in electronic engineering from Tsinghua University, Beijing, China, in 2005 and 2009, respectively.

He is currently an Associate Professor with the Department of Electronic Engineering, Tsinghua University. He has published over 180 peer-reviewed journal and conference papers. He holds over 50 Chinese patents and two PCT patents. His research interests are in the fields of optical wireless communication, wireless communication, intelligent reflecting surface, and integrated sensing and communication.

Dr. Yang received the IEEE Scott Helt Memorial Award (Best Paper Award in the IEEE Transactions on Broadcasting) in 2015. He is the Secretary General of Sub-Committee 25 of the China National Information Technology Standardization (SAC/TC28/SC25). He currently serves as an Associate Editor for the IEEE TRANSACTIONS ON GREEN COMMUNICATIONS AND NETWORKING and *IET Optoelectronics*. He is a Fellow of IET.

Chang Liu received the B.S. degree in communication engineering and the M.S. degree in circuit and system from Beijing Jiaotong University, Beijing, China, in 2012 and 2015, respectively.

He is currently an Associate Researcher with the Center of National Railway Intelligent Transportation System Engineering and Technology as well as with the Signal and Communication Research Institute, China Academy of Railway Sciences Corporation Ltd., Beijing. His research interests are in the field of railway wireless communication technology and system design.

Ling Cheng (Senior Member, IEEE) received the B.Eng. degree (cum laude) in electronics and information from Huazhong University of Science and Technology, Wuhan, China, in 1995, and the M.Ing. degree (cum laude) in electrical and electronics and the D.Ing. degree in electrical and electronics from the University of Johannesburg, Johannesburg, South Africa, in 2005 and 2011, respectively.

In 2010, he joined the University of the Witwatersrand, Johannesburg, where he was promoted to a Full Professor in 2019. He has published more than one hundred research papers in journals and conference proceedings. His research interests are in telecommunications and artificial intelligence.

Prof. Cheng was awarded the Chancellor's medals in 2005 and 2019, and the National Research Foundation ratings in 2014 and 2020. The IEEE ISPLC 2015 Best Student Paper Award was made to his Ph.D. student in Austin. He serves as the Associate Editor for three journals. He has been a Visiting Professor with five universities and the Principal Advisor for over 40 full research postgraduate students. He is the Vice-Chair of IEEE South African Information Theory Chapter.

Jian Song (Fellow, IEEE) received the B.Eng. and Ph.D. degrees in electrical engineering from Tsinghua University, Beijing, China, in 1990 and 1995, respectively.

He is currently the Director of Tsinghua DTV Technology Research and Development Center, Tsinghua University, Beijing. He has been working in quite different areas, including fiber-optic, satellite, and wireless communications, as well as the power-line communications. He holds two U.S. and more than 80 Chinese patents. He has published more than 300 peer-reviewed journal and conference papers and co-authored several books in the aforementioned areas. His current research interest is in the area of digital TV broadcasting, network convergence, and visible light communication networks.

Dr. Song won several awards both international and domestic. He is also a Fellow of IET, Chinese Institute of Electronics, and Chinese Institute of Communications.

Zhu Han (Fellow, IEEE) received the B.S. degree in electronic engineering from Tsinghua University, Beijing, China, in 1997, and the M.S. and Ph.D. degrees in electrical and computer engineering from the University of Maryland at College Park, College Park, MD, USA, in 1999 and 2003, respectively.

From 2000 to 2002, he was a Research and Development Engineer of JDSU, Germantown, MD, USA. From 2003 to 2006, he was a Research Associate with the University of Maryland. From 2006 to 2008, he was an Assistant Professor with Boise State University, Boise, ID, USA. He is currently a John and Rebecca Moores Professor with the Electrical and Computer Engineering Department as well as with the Computer Science Department, University of Houston, TX, USA. His main research targets on the novel game-theory related concepts critical to enabling efficient and distributive use of wireless networks with limited resources. His other research interests include wireless resource allocation and management, wireless communications and networking, quantum computing, data science, smart grid, carbon neutralization, and security and privacy.

Dr. Han received an NSF Career Award in 2010, the Fred W. Ellersick Prize of the IEEE Communication Society in 2011, the EURASIP Best Paper Award for the Journal on Advances in Signal Processing in 2015, the IEEE Leonard G. Abraham Prize in the field of Communications Systems (Best Paper Award in IEEE JSAC) in 2016, the IEEE Vehicular Technology Society 2022 Best Land Transportation Paper Award, and several best paper awards in IEEE conferences. He has been a 1% Highly Cited Researcher since 2017 according to Web of Science. He is also the winner of the 2021 IEEE Kiyo Tomiyasu Award (an IEEE Field Award), for outstanding early to mid-career contributions to technologies holding the promise of innovative applications, with the following citation: "for contributions to game theory and distributed management of autonomous communication networks." He was an IEEE Communications Society Distinguished Lecturer from 2015 to 2018, an ACM Distinguished Speaker from 2022 to 2025, an AAAS Fellow since 2019, and an ACM Fellow since 2024.